N70-35688

NASA CONTRACTOR
REPORT

NASA CR-61332

ANALYSIS OF EXHAUST PLUMES FROM SKYLAB-CONFIGURATION R-4D ATTITUDE CONTROL MOTORS

By A. W. Ratliff, B. J. Audeh, and D. D. Thornhill

Lockheed Missiles and Space Company
Huntsville Research and Engineering Center
Huntsville Research Park, 4800 Bradford Dr.
Huntsville, Alabama

March 1970

Prepared for

NASA-GEORGE C. MARSHALL SPACE FLIGHT CENTER
Marshall Space Flight Center, Alabama 35812

1. Report No.	2. Government Accession No.	3. Recipient's Catalog No.
CR-61332		

4. Title and Subtitle	5. Report Date
ANALYSIS OF EXHAUST PLUMES FROM SKYLAB-CONFIGURATION R-4D ATTITUDE CONTROL MOTORS	March 1970
	6. Performing Organization Code
7. Author(s) A. W. Ratliff, B. J. Audeh, D. D. Thornhill	8. Performing Organization Report No. HREC/20082-22, LMSC/HREC D162171
9. Performing Organization Name and Address: Lockheed Missiles & Space Company, Huntsville Research & Engineering Center, Huntsville Research Park, 4800 Bradford Drive, Huntsville, Alabama	10. Work Unit No.
	11. Contract or Grant No. NAS8-20082
12. Sponsoring Agency Name and Address: NASA-Marshall Space Flight Center, Marshall Space Flight Center, Alabama, 35812	13. Type of Report and Period Covered: Contractor Report
	14. Sponsoring Agency Code

15. Supplementary Notes

16. Abstract

The exhaust plume flow field of the Skylab (formerly AAP) configuration reaction control system (RCS) engines has been determined analytically as a preliminary step in the prediction of heating rates, forces, and contamination effects due to these plumes. The engine used, designated R-4D, burns nitrogen tetroxide and monomethylhydrazine (N_2O_4/MMH) propellant. Engine configurations, nozzle geometries, propellant description, and operating conditions were supplied by MSFC, Huntsville, Alabama; the Marquardt Corp., Van Nuys, California; and MSC, Houston, Texas. Plume flow fields in a vacuum environment were calculated for the engine used on the Command Service Module. Calculations began in the combustion chamber, extended through the nozzle, and continued into the plume to about 50 feet axially and radially from the engine. Flow striations (oxidizer-to-fuel variations) were considered in the analysis based on injector information supplied by MSC. A thermochemical program was used to define combustion product species concentrations and thermodynamic properties of the propellant system. A one-dimensional streamtube solution was used to define the physical and thermodynamic properties after equilibrium combustion. An equilibrium chemistry ducted mixing analysis was made through the combustion chamber. A time-dependent transonic solution was used to describe the two-dimensionality of the flow in the convergent section of the nozzle and through the nozzle throat. A method-of-characteristics solution was begun at the nozzle throat using equilibrium thermochemical properties up to a point in the flow at which a kinetic analysis indicated that the flow was chemically frozen. The plume was then generated using the nozzle exit conditions as starting information. The nozzle boundary layer effect on the plume was included and the region where non-continuum conditions may exist is indicated. Two shock waves were considered and treated in this analysis. The nozzle shock and its reflection from the nozzle axis were computed as integral parts of the total flow field. Also included in this analysis is a correlation study of several R-4D engine and plume parameters. This information provides justification for the particular oxygen-to-fuel gradient used as well as verification of the general analysis procedure.

17. Key Words (Suggested by Author(s))	18. Distribution Statement
	PUBLIC RELEASE E. D. GEISSLER, Dir, Aero-Astrodynamics Lab, MSFC

19. Security Classif. (of this report)	20. Security Classif. (of this page)	21. No. of Pages	22. Price*
Unclassified	U	57	

*For sale by the Clearinghouse for Federal Scientific and Technical Information Springfield, Virginia 22151

FOREWORD

This report presents the results of work performed by Lockheed's Huntsville Research & Engineering Center while under subcontract to Northrop Nortronics (NSL PO 5-09287) for the Aero-Astrodynamics Laboratory of Marshall Space Flight Center (MSFC), Contract NAS8-20082. This task was conducted in response to the requirement of Appendix B-1, Schedule Order No. 147 under the technical cognizance of Homer B. Wilson, Jr., Terry F. Greenwood and David C. Seymour.

ACKNOWLEDGMENT

The authors wish to acknowledge the contribution of Joseph L. Sims of the Fluid Mechanics Research Office of the Aero-Astrodynamics Laboratory (MSFC), for helpful consultations during portions of this study.

SUMMARY

The exhaust plume flow field of the Skylab (formerly AAP) configuration reaction control system (RCS) engines has been determined analytically as a preliminary step in the prediction of heating rates, forces and contamination effects due to these plumes. The engine utilized, which is designated R-4D, burns nitrogen tetroxide and monomethlyhydrazine (N_2O_4/MMH) propellant.

Engine configurations, nozzle geometries, propellant description, and operating conditions were supplied by three agencies: (1) NASA-Marshall Space Flight Center, Huntsville, Alabama; (2) the Marquardt Corporation, Van Nuys, California; and (3) NASA-Manned Spacecraft Center, Houston, Texas.

Plume flow fields in a vacuum environment were calculated for the engine used on the Command Service Module. Calculations began in the combustion chamber extended through the nozzle and continued into the plume to about 50 feet axially and radially from the engine.

Flow striations (oxidizer-to-fuel variations) were considered in the analysis based on injector information supplied by the Manned Spacecraft Center. A thermochemical program was used to define combustion product specie concentrations and thermodynamic properties of the propellant system. A one-dimensional streamtube solution was used to define the physical and thermodynamic properties after equilibrium combustion. An equilibrium chemistry ducted mixing analysis was made through the combustion chamber. A time-dependent transonic solution was used to describe the two dimensionality of the flow in the convergent section of the nozzle and through the nozzle throat. A method-of-characteristics solution was begun at the nozzle throat using equilibrium thermochemical properties up to a point in the flow at which a kinetic analysis indicated that the flow was chemically frozen. The plume was then generated using the nozzle exit conditions as starting information. The nozzle

boundary layer effect on the plume was included and the region where non-continuum conditions may exist is indicated.

Two shock waves were considered and treated in this analysis. The nozzle shock and its reflection from the nozzle axis were computed as integral parts of the total flow field. Also included in this analysis is a correlation study of several R-4D engine and plume parameters. This information provides justification for the particular oxygen-to-fuel gradient used as well as verification of the general analysis procedure.

CONTENTS

LIST OF ILLUSTRATIONS

LIST OF ILLUSTRATIONS (Continued)

Section 1
INTRODUCTION

When attitude control maneuvers are required for the Skylab configuration, small reaction motors are employed to effect these maneuvers. Two separate reaction control systems are utilized in the Skylab configuration: (1) the Auxiliary Propulsion System (APS) which is located on the aft end of the S-IVB Orbital Workshop; (2) a reaction control system (RCS) on the Command Service Module (CSM). When some of the motors of these systems are operated, various parts of the overall configuration may be subjected to direct or indirect impingement of the exhaust plume from the operating engine. An analysis of the Wet Workshop APS system engine is contained in Ref. 1. This report is concerned with the Marquardt R-4D engine used on the CSM.

The effects of plume impingement should be carefully assessed with respect to possible adverse forces and heating rates which may arise. The forces must be evaluated in order to determine system size and duty cycle as well as for structural loading effects. The heating rates due to impingement on various parts of the vehicle are also an important consideration. Some parts of the vehicle may have temperature-sensitive components for which the environment must be known in order to protect them properly. Another effect which must be evaluated is concerned with the possible contamination which may occur on the portions of the vehicle subject to plume impingement. It is important to be able to predict any changes which the vehicle surfaces may undergo due to the adverse rocket plume environment. Temperature control devices, for example, are dependent upon their surface optical properties for effective operation. Thus, if contamination changes these properties, the effective use of the device may be compromised.

In view of the many problems which arise due to plume impingement, it is important to predict adequately the resulting effect on a particular vehicle or portion of a vehicle. In order to make predictions of plume impingement

effects; an accurate and detailed description of the plume must be available. It is the purpose of the study reported herein to provide the analytical description of plumes from the Skylab configuration Reaction Control System motors (R-4D) so that their effects on the vehicle can be analyzed. The data presented in this report are for free plumes exhausting into a vacuum environment and do not include the impingement effects per se, but provide basic information necessary for conducting impingement analyses.

Section 2
METHOD OF ANALYSIS

The importance of plume impingement with respect to the Skylab configuration dictates that the plume data utilized be as detailed as possible. Since there are numerous methods for analyzing plumes based upon various assumptions, the methodology used in this study is discussed in some detail.

2.1 COMBUSTION CHAMBER AND NOZZLE THROAT

The calculational procedure was begun with a combustion chamber analysis consisting of a streamtube combustion solution (Ref. 2) coupled with an equilibrium, ducted, mixing calculation (Ref. 3). Because radial mixture ratio gradients were present, variations in the combustion gas properties were accounted for by using a number of streamtubes each with a different mixture ratio. The solution assumed the gases to be in chemical equilibrium. No radial pressure gradients were allowed, and the inlet conditions at the injector face were determined by the extensive correlation study discussed in the Appendix.

The Streamtube program (Ref. 2) was used to determine the physical and thermodynamic properties after equilibrium combustion to provide data for the ducted equilibrium mixing program (Ref. 3). The equilibrium mixing calculation was done for the flow through the combustion chamber, and the resultant properties at the entrance to the convergent section were used in the transonic solution. The transonic region of the R-4D engine was analyzed using a Lax-Wendroff-type of time-dependent solution. The two-dimensional effects are thus included in the transonic calculations. The program treats flows with oxidizer-to-fuel (O/F) gradients, and real gas equilibrium processes were used. The transonic program generated a starting line, i.e., initial conditions, for beginning a method-of-characteristics (MOC) calculation for the nozzle expansion section. The starting line derived in this fashion accounts

for combustion chamber momentum loss and radial flow striations, but does not account directly for combustion efficiency. Boundary layer and wall heat transfer in the combustion chamber were also neglected.

2.2 NOZZLE EXPANSION

Once the nozzle throat conditions were known, a MOC calculation was used to analyze the supersonic flow downstream of the throat. The Lockheed Method-of-Characteristics Computer Program (Ref. 4) was used to accomplish all the supersonic calculations for this study. The basic program of Ref. 4 was specially modified to handle the flow striations which existed in the engines. Initially, the flowfield chemistry was assumed to be in equilibrium and the gas properties were obtained from the NASA-Lewis Research Center Thermochemical program (Ref. 5). To determine the chemical reaction freeze point, the pressure distribution along the nozzle wall and centerline obtained from the chemical equilibrium solution were used as boundary conditions for a one-dimensional calculation using finite rate chemistry (Ref. 6). The streamlines analyzed in each case consisted of the nozzle centerline and the wall contour. When the "freeze" points were determined from the finite-rate analysis, the thermochemistry data were regenerated using the pressure freeze option of the NASA-Lewis program (Ref. 7). This option allows the thermochemical calculations to switch from equilibrium to frozen at a specified pressure which was obtained from the kinetics analysis of Ref. 6. The equilibrium/frozen gas properties were then used in a second calculation of the nozzle flow field which approximately accounted for the finite-rate effects on the resulting flow field. Because mixture ratio gradients were present, each streamline was analyzed at its own local O/F value and the "freeze points" on streamlines between the centerline and nozzle wall were assumed to vary linearly with O/F ratio.

2.3 NOZZLE SHOCK WAVES

Most contoured nozzles give rise to the formation of an internal shock wave. The shock is initiated by a discontinuity in the second derivative of the contoured nozzle at the junction between the expansion section, near the nozzle

throat, and the recurved section which comprises the remainder of the nozzle. This shock is generally weak at its origin and gradually increases in strength, becoming quite strong as it intersects the nozzle axis of symmetry. A detailed description of the plume requires that the effect of this shock on the local flow properties be taken into account. Thus in keeping with the study objective, this shock wave was computed as an integral part of the nozzle flowfield analysis.

When shock waves, in general, approach the nozzle axis of symmetry, two things may happen. First, if the shock is strong enough, a Mach disk may form which causes the flow to "shock down" into the subsonic regime. Weaker shocks, however, may go through a regular reflection, at least in an inviscid analysis, such that the flow remains supersonic even behind the reflected leg of the shock system. Shock waves encountered in the nozzles of this study were weak and reflected regularly at the axis.

2.4 PLUME ANALYSIS

When the nozzle solution was completed, including the incident nozzle shock, the analysis was continued into the plume flow field. The initial conditions, i.e., start line, for the plume analysis consisted of the downstream shock points from the nozzle analysis. However, because the shock itself does not progress all the way to the nozzle wall, other points from the nozzle analysis were also required. These points consisted of flowfield data points proceeding from the shock wave, across the nozzle exit plane, to the nozzle lip. The flowfield chemistry used by the plume analysis was the same as that used for the nozzle. This was possible because the kinetics analysis had indicated that the flowfield chemistry was frozen inside the nozzle and, since the flow continually expands into the plume, the chemistry should then, remain frozen.

When the procedure was restarted to generate the plume, the incident nozzle shock was reflected from the nozzle axis and continued throughout the plume. The plume was allowed to expand to a vacuum environment as a boundary condition. This is, of course, quite impractical in a numerical solution,

because of the extremely high Mach numbers and pressures which approach zero. To circumvent the numerical problems, the expansion was only allowed to approach the limiting expansion angle within 10 deg and the solution was stopped at that point.

2.4.1 Non-Continuum Effects

When a plume expands into a vacuum, its density eventually becomes so low that the flow no longer obeys continuum gas dynamics laws. Ideally, plume calculations should consider non-continuum effects (Ref. 8). Continuum analyses, for instance, should be stopped when the flowfield parameters and gradients satisfy the Knudsen number criteria for free molecular flow, i.e., vibrational, rotational and translational energy modes "frozen". The calculations should then be continued along streamlines from an apparent source, assuming that the streamlines remain straight and the molecular velocities are all in the direction of the flow. In the free molecular regime, therefore, the stream velocity is constant and the density varies in inverse proportion to the cross-sectional area of the stream tube. For the analysis reported here, continuum gas dynamic relations were employed throughout the flow. Except for deviation of the translational temperature, as the flow approaches free molecular conditions, the continuum analysis is a good approximation. A physical explanation of this phenomenon is that in using the method-of-characteristics continuum analysis the angle between the streamlines and the Mach lines becomes very small, such that there is little lateral interaction between streamlines, thus approximating free-molecule flow. A calculation was performed, however, of the location of the translational "freezing" line to indicate incipient free-molecule flow.

2.4.2 Nozzle Wall Boundary Layer

Several recent studies have indicated that the presence of a nozzle wall boundary layer can have a significant effect on the local exhaust plume properties. Boynton in Ref. 9 discusses the inviscid expansion of nozzle boundary

layers from various engines ranging in thrust from 10 lb to 80,000 lb. His calculations indicate deviations which increase with expansion angle. Above 75 degrees expansion angle, for instance, differences in dynamic pressure of a factor of 10 were found.

Another nozzle wall boundary layer investigation was carried out in Ref. 10. A typical small RCS engine was analyzed with and without the boundary layer. Every input parameter, as well as the characteristic mesh size, was identical so that the boundary layer effect was the only difference between the two cases. As in Ref. 9, this study shows significant variations in the plume due to the boundary layer, especially in the outer 50% of the flow.

In light of these studies, the nozzle wall boundary layer was included in the present study, and its effect is inherent in the results presented in this report.

2.4.3 Condensation

The condensed form of the species present in the exhaust plume was not considered by the thermochemical or the flowfield analysis. Because of this, vapor pressure data for the various species were examined to determine if condensation could occur in the plume. Conditions in the continuum region which could lead to the formation of condensed H_2O were noted to exist for flows of Mach 10.0 and higher. Conditions favorable to the condensation of CO_2 exist for flows of Mach 15.0. Conditions favorable to the condensation of CO and N_2 exist for flows of Mach 29.0. Condensation will probably not occur for H_2. Solid particles may exist for the CO_2 and H_2O downstream of the region where conditions for the condensation are favorable. Due to the high velocities which exist in the plume flow field, condensed species may or may not be formed in the plume region shown. Incipient condensation and the calculation of a multi-phase plume flow field was not considered in this analysis.

2.4.4 Accuracy of the Predicted Plume Envionment

Determining a quantitative value for relating the accuracy of a rocket exhaust plume environment is a complex problem, involving numerous considerations. A detailed evaluation of plume environment accuracy is presented in Ref. 11 and can be used to estimate the gross accuracy of plume flow field parameters.

Section 3
DISCUSSION

For the R-4D engine analyzed, approximately 24 percent of the fuel is used for film cooling the engine and nozzle walls. Although this provides an excellent heat barrier, the practice severely reduces engine performance. In addition, its effect is propagated into the plume, which creates regions of varying mixture ratio with attendant variations of thermodynamic and gas dynamic parameters.

Experimental tests of the R-4D engine conducted by NASA-Manned Spacecraft Center resulted in a specific impulse of about 285 sec. One-dimensional adiabatic flame temperature equilibrium calculations by the NASA-Lewis Thermochemical program showed a specific impulse of 337 sec. The difference in specific impulse values are attributed to inefficiencies which reduce the performance of the engines below the maximum energy available from the propellants. Several causes of non-ideal performance have been isolated, for instance: momentum loss because of combustion, O/F maldistribution, kinetic effects and two dimensional effects. These conditions still do not account for the entire performance loss of the engine. The remaining losses are attributed to the inefficiencies in the combustion process.

The ICRPG Committee (Ref. 12) has recommended a method of artificially reducing propellant heats of formation to account for combustion inefficiencies. A dual study of the R-4D was therefore conducted. The standard heat of formation was used in one case and the heat of formation reduced by 250 cal/gm in the other case. The 250 cal/gm was an arbitrary value selected to approximate the experimental I_{sp} value. Loss mechanisms discussed previously were included in both analyses. Only the standard heat of formation case is presented here in order to provide conservative design parameters.

In this analysis several of the loss mechanisms are inherent. The O/F gradient effect, the momentum loss in the combustion process, two-dimensional effects in the transonic and supersonic flow portions of the engine were treated as integral parts of the analysis. The finite-rate effects were treated by an equilibrium/frozen approximation procedure. A parametric variation was done of the freezing point pressure used in the equilibrium/frozen nozzle flow calculations. The effect of location of the freezing point on the predicted I_{sp} was found to be very small (Ref. 13). For extreme cases such as freezing the flow at the throat, the I_{sp} was reduced by 5 percent. Any of the freezing pressure values within the range of selection showed a negligible variation in the predicted I_{sp} value.

3.1 COMBUSTION ANALYSIS

Prior to performing the calculations reported in the main body of this report, a correlation study of the R-4D engine using N_2O_4/A-50 propellants was performed. Experimental data in the form of pitot pressures, heating rates and performance were available which were used, along with injector geometry, to determine mass flow and O/F ratio distributions. A detailed discussion of this auxiliary study is contained in the Appendix. Figure 1 shows a sketch of the R-4D Rocket Engine.

The combustion analysis for N_2O_4/MMH propellants was conducted based on the mixture ratio-mass flow distribution for N_2O_4/A-50 propellants, (see Appendix) and the method of analysis described in Section 2.

An assumption of uniform mass flow per unit area over the entire injector face was made to eliminate severe step gradients in mass flow-mixture ratio due to injector geometry. This assumption was necessary to obtain a physically reasonable solution of the initial combustion process from the Streamtube program. The proper overall mass flow was maintained, but the exact mass flow through the preigniter region could not be matched using this assumption.

Orifice(s)	$\dot{m}$ in lb/sec		O/F	% Fuel in Terms of Total Fuel	% Fuel in Terms of Total Propellant
	ϕ Oxidizer	F Fuel			
Doublet Inside Preigniter	0.061	0.0175	3.47	14.0	4.8
Preigniter Cooling	0.0	0.0169	0.0	13.5	4.7
Main Core Doublet	0.180	0.061	2.96	48.5	17.0
Wall Cooling	0.0	0.030	0.0	24.0	8.3

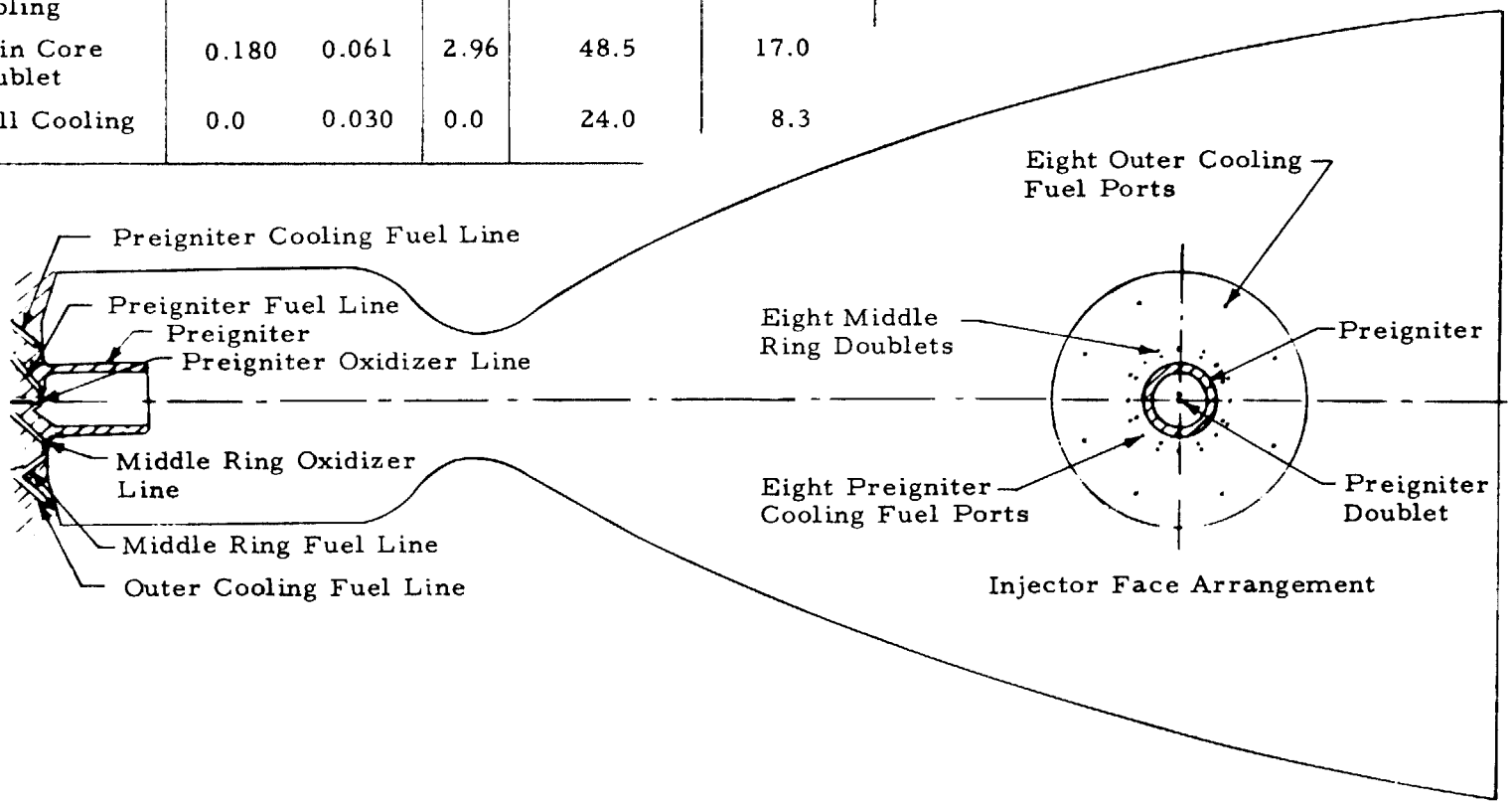

Fig. 1 - Sketch of the R-4D Rocket Engine

The initial O/F ratio distribution across the injector face, based on the preceding discussion plus the assumption of a parabolic shape, is the following:

$$\text{O/F ratio} = 3.5 - 3.76\,r^2$$

where the dimensions of r are inches.

The Streamtube program provided data for the Ducted Equilibrium Mixing program. The velocity, temperature and O/F ratio distributions at the injector after the equilibrium combustion and those at the entrance to the convergent section are shown in Fig. 2. From these results it was concluded that a small amount of mixing occurred through the chamber length. This was the result of the low value of constant viscosity model chosen (6.033×10^{-4} slugs/ft-sec) and because partial mixing had been presumed with the introduction of uniform mass flow per unit area across the injector face.

3.2 TRANSONIC ANALYSIS

The nozzle contour, Fig. 3, used for this analysis was obtained from the Marquardt Corporation. The points from Table 1 were curve-fit by a least-squares technique and the two resulting curves then used as upper boundary conditions in the transonic and the MOC solutions.

$$0 \leq X \leq 0.278$$

$$R = -1.0\left(\sqrt{0.27931 - X^2} - 0.9625\right)$$

$$0.278 \leq X \leq 6.984$$

$$R = -0.000256\,X^4 + 0.0058873\,X^3 - 0.074477\,X^2 + 0.66247\,X + 0.33698$$

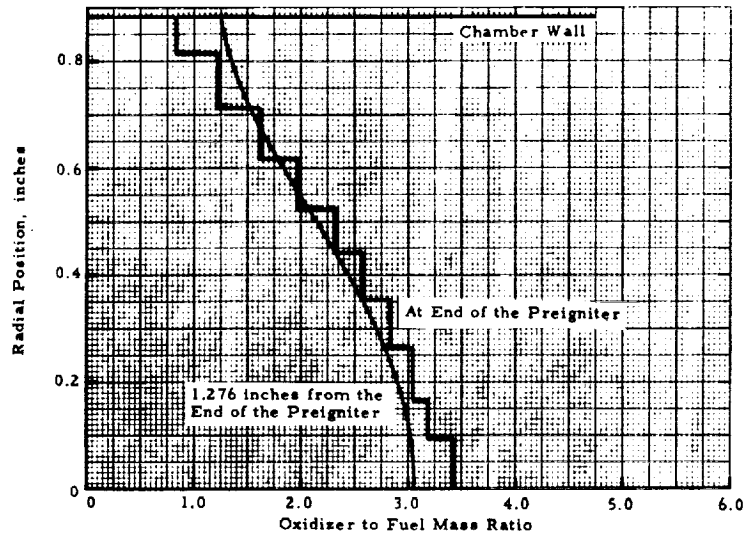

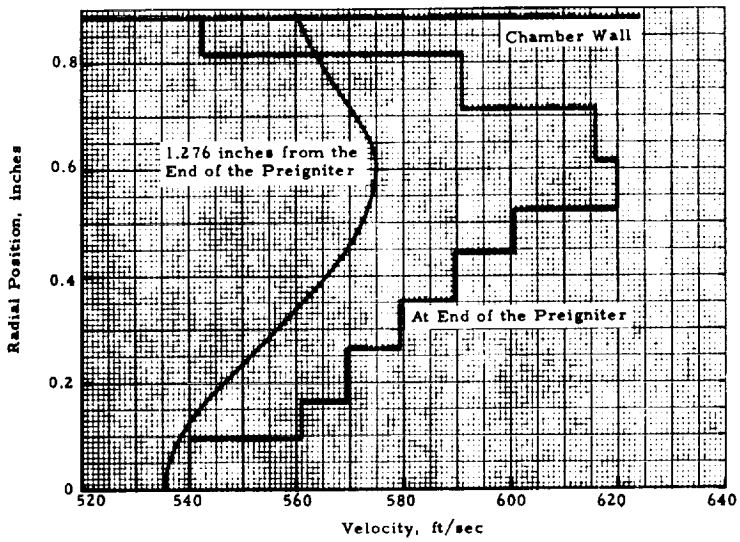

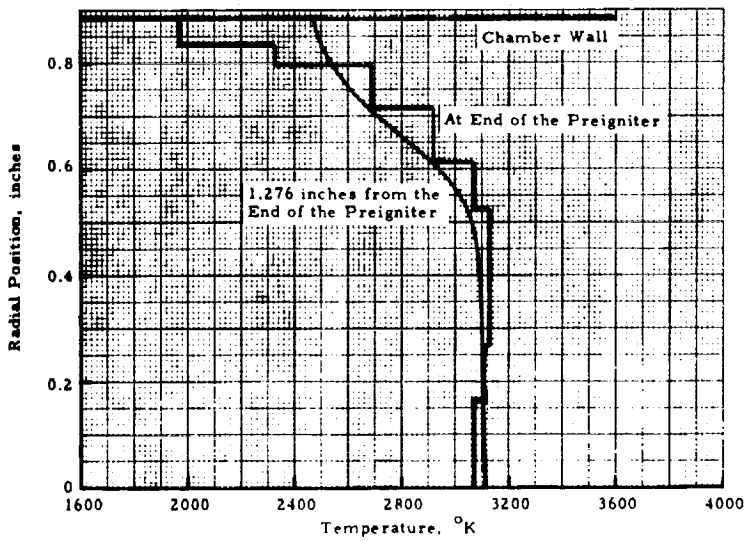

Fig. 2 - Properties at the End of the Preigniter and at the Inlet to the Convergent Section of the Nozzle (1.276 inches from the end of the Preigniter)

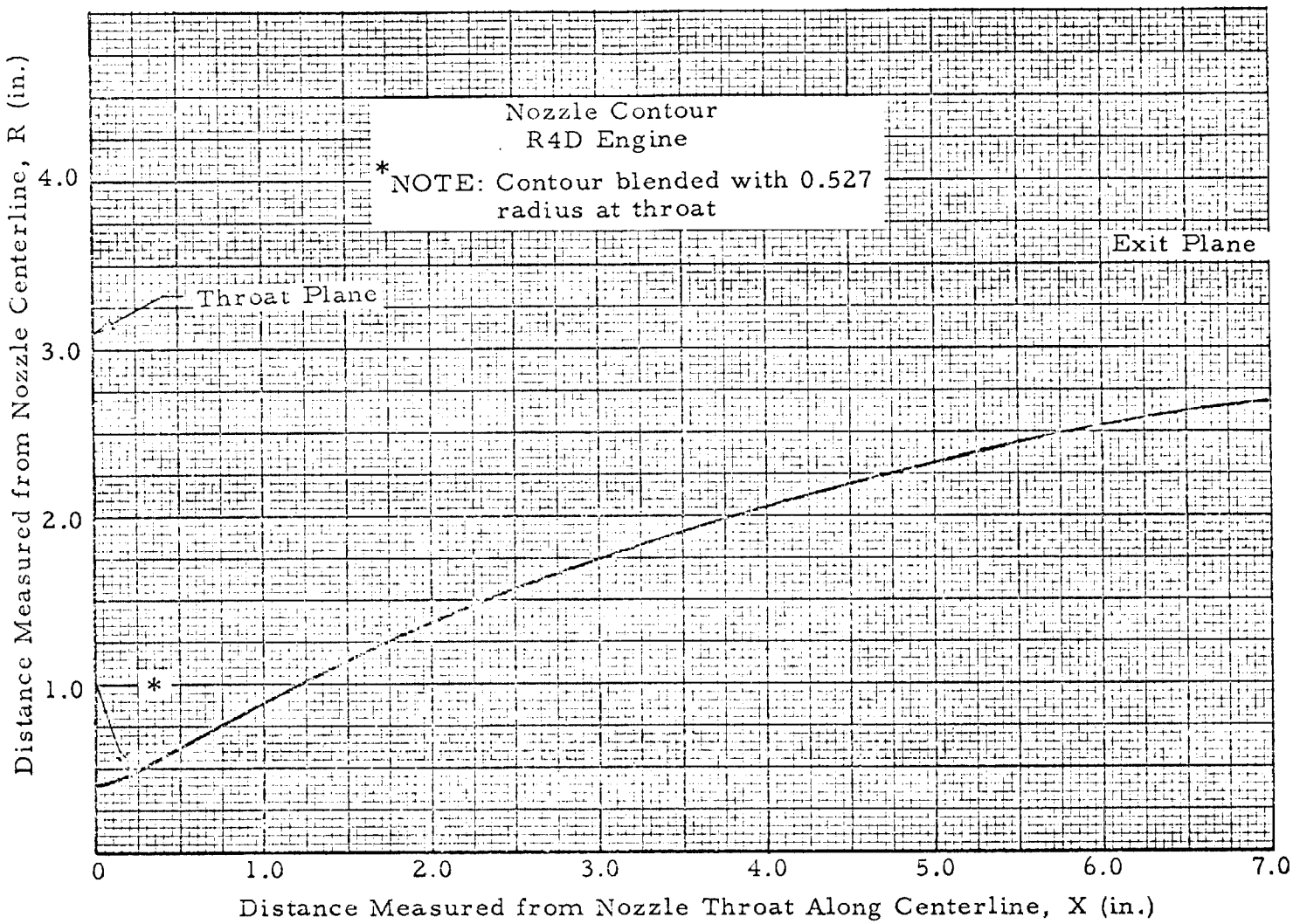

Fig. 3 - Nozzle Contour for R4D

Table 1

NOMINAL R-4D ENGINE OPERATING CHARACTERISTICS FOR COMMAND SERVICE MODULE REACTION CONTROL SYSTEM APPLICATION

Propellant	Engine Parameters
Oxidizer N_2O_4 Fuel $CH_3 NHNH_2$ (Monomethylhydrazine)	$A/A^* = 40.0$ $D_{exit} = 5.46$ in. $\Theta_{exit} = 8$ deg $P_C = 100$ psia $O/F = 2.03 \pm 0.03$ $\dot{m}_{total} = 0.366$ lb_m/sec Thrust (nominal) $= 100 \pm 5$ lb_f(vac) $D_{chamber} = 1.77$ in.

Nozzle Contour		
X	R	
0.000	0.434	Throat – Blend nozzle
0.278	0.513	contour with throat
0.474	0.635	using 0.527 radius of
0.812	0.832	curvature. See Fig. 3.
1.339	1.106	
1.400	1.134	
1.866	1.349	
2.393	1.565	
2.920	1.762	
3.447	1.940	
3.974	2.101	
4.501	2.245	
5.028	2.372	
5.555	2.483	
6.082	2.583	
6.609	2.671	
6.984	2.730	Exit Plane

An unsteady time-dependent finite difference solution procedure was used to describe the transonic flow in the nozzle throat region. Initial conditions consisted of the mixed profiles of the gas dynamic properties at the entrance to the convergent section (Fig. 2). Non-isoenergetic flow was considered (i.e., O/F gradients) as well as equilibrium chemistry throughout the transonic region. Supersonic starting conditions for the MOC program were obtained from the transonic flow description. The Mach number, flow angle and O/F ratio distribution on the starting line are shown in Fig. 4. (See Table 1 for a description of the operating characteristics of the R-4D engine.)

3.3 NOZZLE FREEZING POINTS

The variable O/F MOC program was used to describe the flow field within the nozzle and plume regions. The AeroChem Finite-Rate program was applied to determine the freezing points for the centerline and wall streamlines. The values of freeze pressure were determined by plotting the variation of the constituents along the centerline and wall of the nozzle. The mole fraction variation of the constituents along the centerline of the R-4D nozzle are shown in Fig. 5. The region where there is negligible change in the mole fraction of the constituents is defined as a transition zone from fast (nearly equilibrium) to slow (nearly frozen) reactions. For computational purposes the zone is shrunk to a point (the freezing point). The pressure corresponding to that axial location becomes the freezing pressure. The O/F ratio of 3.07 on the centerline was frozen at 0.008 atmospheres of pressure while the O/F ratio of 1.24 on the wall was frozen at 3.0 atmospheres. The freezing pressure used for the O/F ratios other than those on the centerline and wall was taken as the value obtained by a straight-line variation between the calculated wall and centerline values. Since no practical means was available to determine the freezing point values for the intermediate O/F ratios and any variation chosen was arbitrary, the use of the least confusing straight-line variation seemed appropriate. The final nozzle flow calculation was done using the equilibrium/frozen thermochemical properties shown in Table 2.

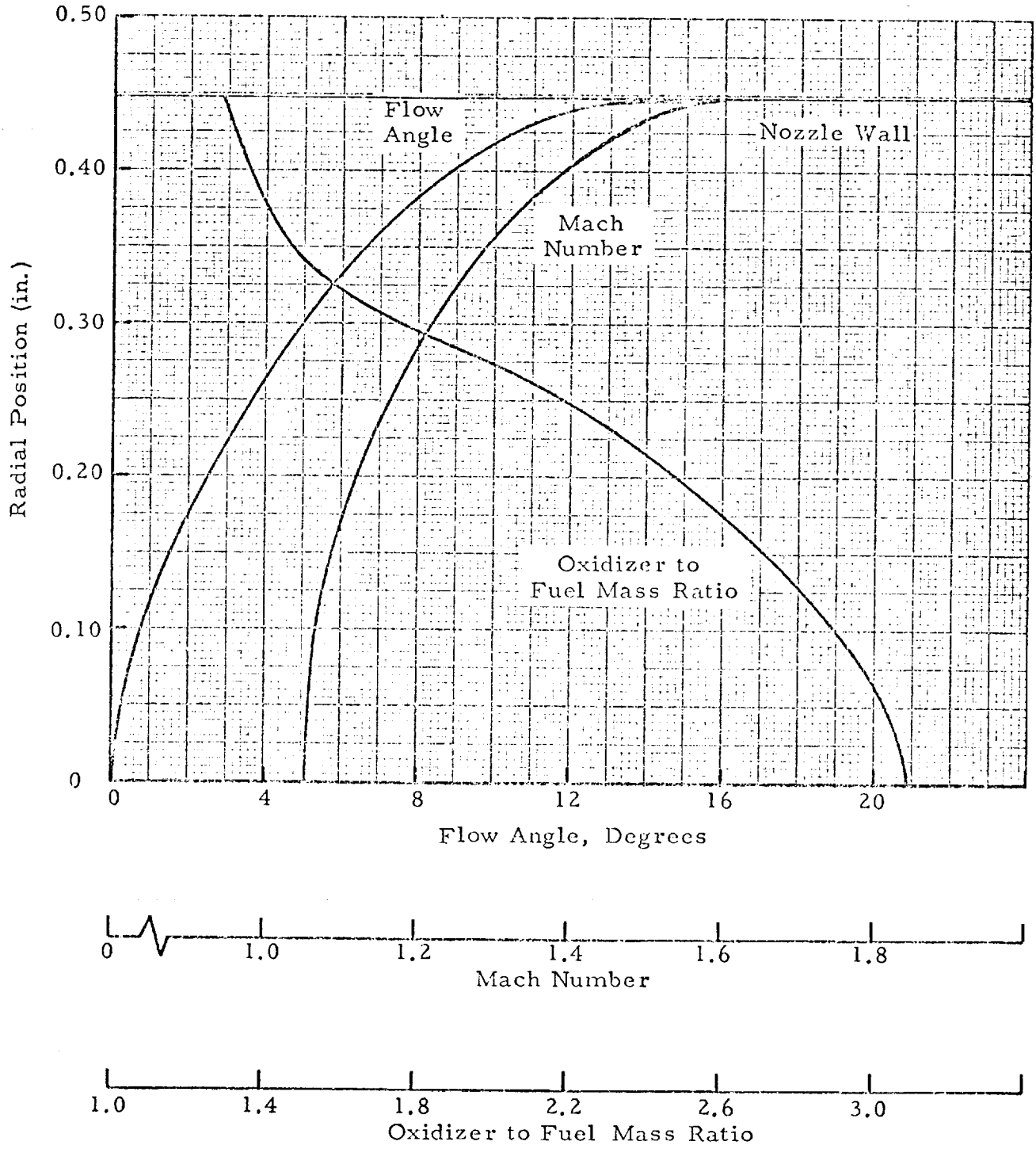

Fig. 4 - Starting Line Conditions for MOC Calculation.
Starting Line at 0.124 in. from Throat.

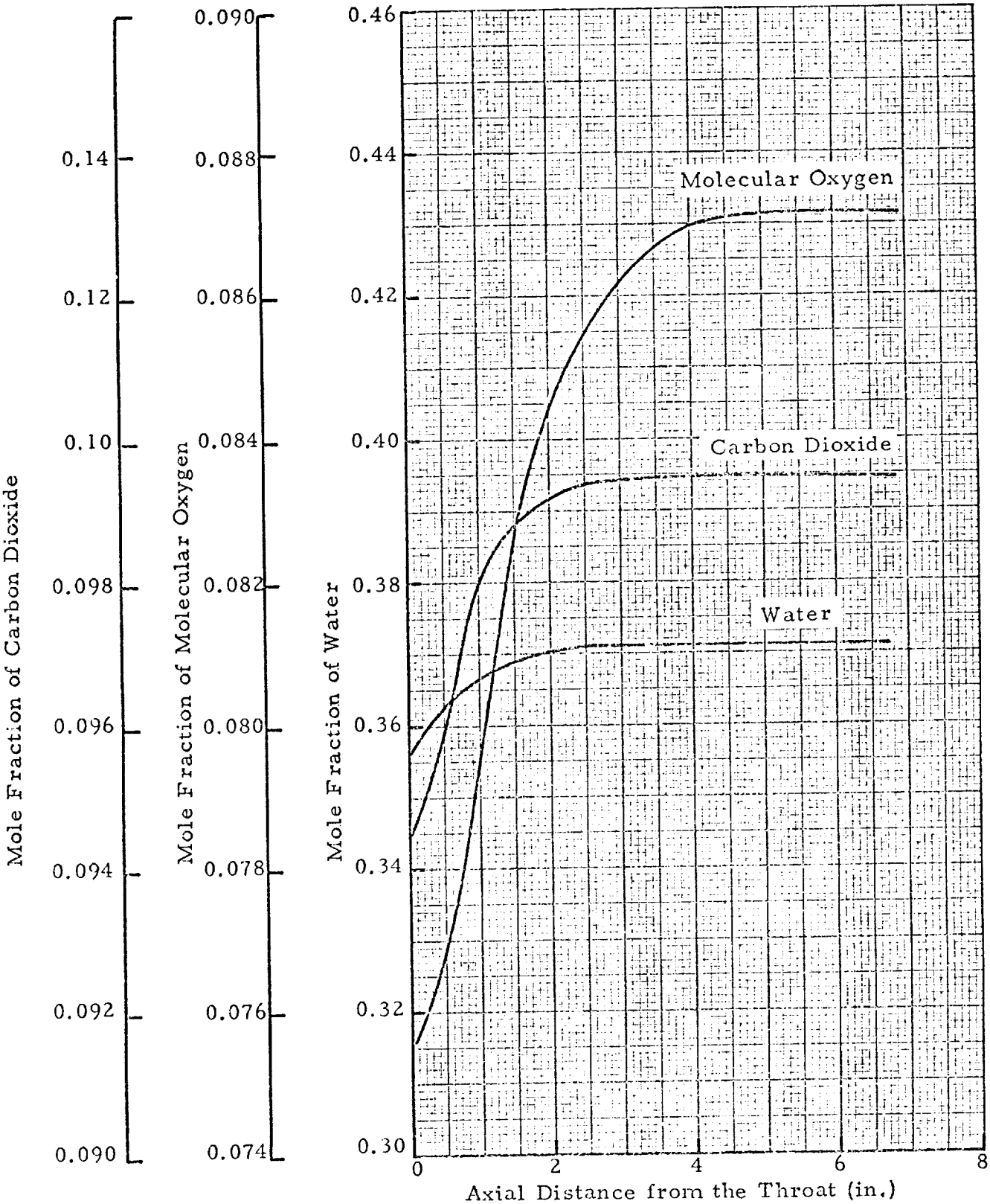

Fig. 5a - Constituent Mole Fraction Variation Along the Centerline of the R-4D Engine Nozzle at an O/F of 3.07 for an MMH/N_2O_4 Propellant System.

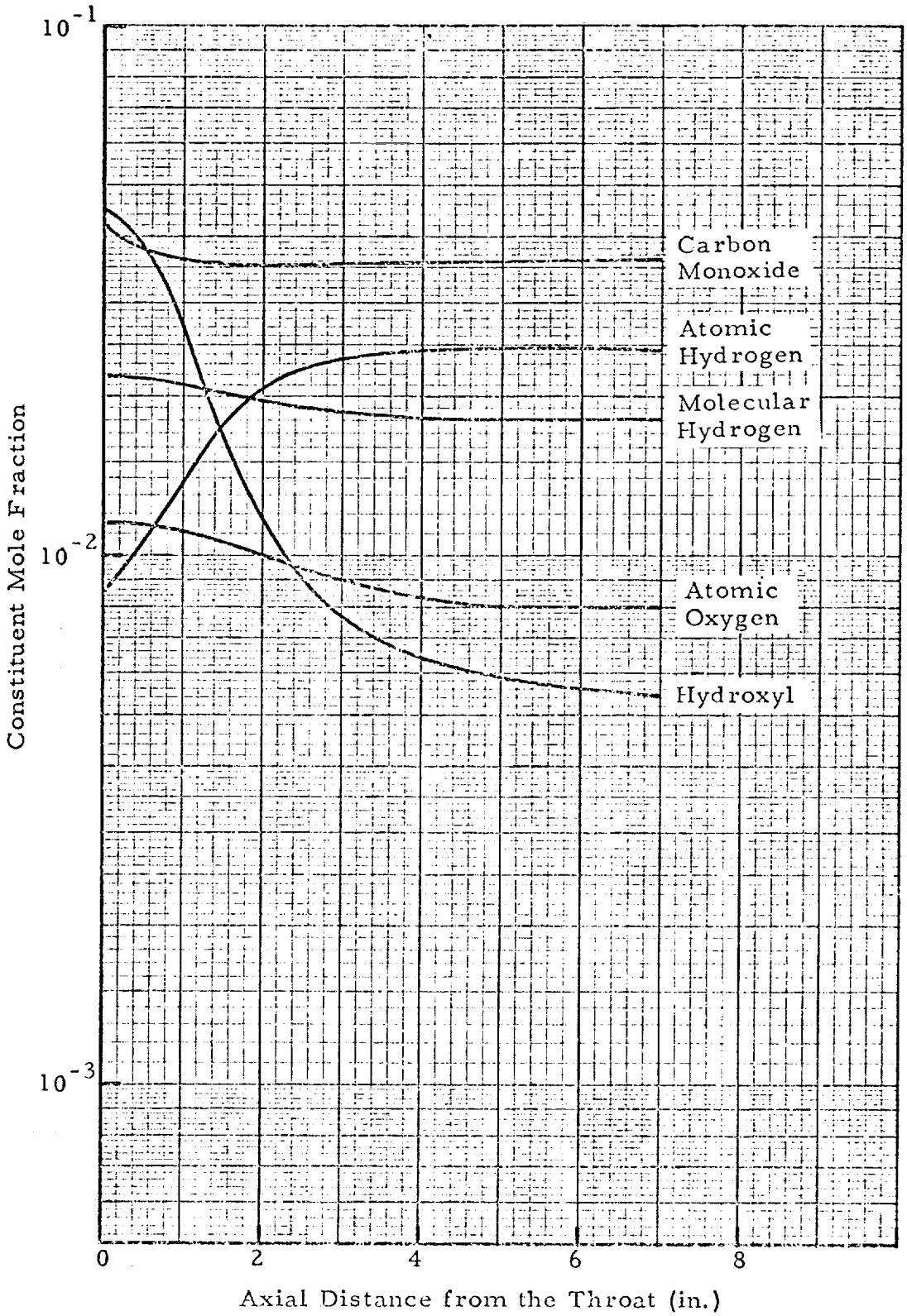

Fig. 5b - Constituent Mole Fraction Variation Along the Centerline of the R-4D Engine Nozzle at an O/F of 3.07 for an MMH/N_2O_4 Propellant System.

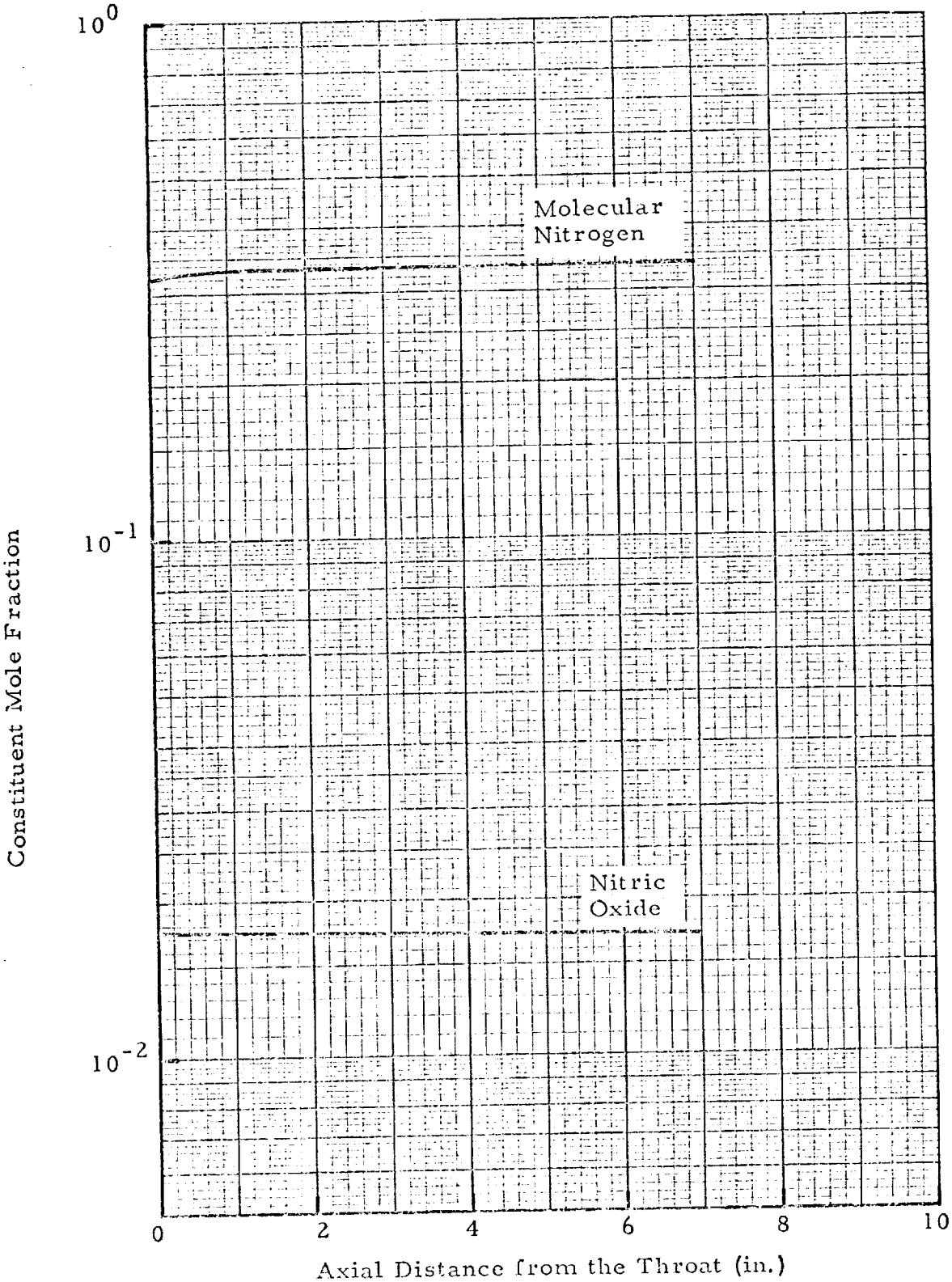

Fig. 5c - Constituent Mole Fraction Variation Along the Centerline of the R-4D Engine Nozzle at an O/F of 3.07 for an MMH/N_2O_4 Propellant System.

THE FOLLOWING GAS PROPERTIES IN ENGLISH UNITS ARE FOR MONOMETHYLHYDRAZINE/NITROGEN TETROXIDE

Table 2
THERMODYNAMIC PROPERTIES OF AN EQUILIBRIUM/FROZEN MONOMETHYLHYDRAZINE/NITROGEN TETROXIDE SYSTEM FOR THE OXIDIZER-TO-FUEL MASS RATIO RANGE OF THE R-4D ENGINE

REAL GAS PROPERTIES

O/F	S	R	GAMMA	T	P
0.150000E 01					
	0.000000E-38				
		0.[illegible]E-38	0.297225E 04	0.124981E 01	0.921846E 04	0.144000E 05
		0.[illegible]E 04	0.296936E 04	0.126611E 01	0.372206E 04	0.778838E 04
		0.[illegible]E 04	0.296930E 04	0.126768E 01	0.366166E 04	0.720000E 04
		0.[illegible]E 04	0.296930E 04	0.126767E 01	0.366166E 04	0.720000E 04
		0.[illegible]E 04	0.296930E 04	0.126812E 01	0.340425E 04	0.514296E 04
		0.[illegible]E 04	0.296930E 04	0.128665E 01	0.319966E 04	0.360000E 04
		0.[illegible]E 04	0.296930E 04	0.129865E 01	0.272027E 04	0.189476E 04
		0.[illegible]E 04	0.296930E 04	0.133607E 01	0.134786E 04	0.106676E 03
		0.[illegible]E 04	0.296930E 04	0.137526E 01	0.822066E 03	0.167446E 02
		0.[illegible]E 04	0.296930E 04	0.137676E 01	0.784960E 03	0.141176E 02
		0.[illegible]E 04	0.296930E 04	0.138406E 01	0.582776E 03	0.479966E 01
		0.[illegible]E 04	0.296930E 04	0.139356E 01	0.264856E 03	0.287816E 00
	0.206636E 05				
		0.000000E-38	0.301956E 04	0.115726E 01	0.388356E 04	0.143906E 02
		0.[illegible]E 04	0.299437E 04	0.118306E 01	0.360886E 04	0.816866E 01
0.175000E 01					
	0.000000E-38				
		0.000000E-38	0.252816E 04	0.116846E 01	0.528396E 04	0.144000E 05
		0.396556E 04	0.250716E 04	0.118406E 01	0.484016E 04	0.778836E 04
		0.419466E 04	0.250506E 04	0.118656E 01	0.480536E 04	0.720006E 04
		0.504816E 04	0.249726E 04	0.119776E 01	0.456616E 04	0.514296E 04
		0.504706E 04	0.249726E 04	0.124236E 01	0.456616E 04	0.514296E 04
		0.577506E 04	0.249726E 04	0.124546E 01	0.425776E 04	0.360006E 04
		0.679396E 04	0.249726E 04	0.125196E 01	0.374706E 04	0.189476E 04
		0.930776E 04	0.249726E 04	0.129556E 01	0.202686E 04	0.106676E 03
		0.100916E 05	0.249726E 04	0.133216E 01	0.130256E 04	0.167446E 02
		0.101456E 05	0.249726E 04	0.133536E 01	0.124806E 04	0.141176E 02
		0.104316E 05	0.249726E 04	0.135266E 01	0.946736E 03	0.479966E 01
		0.109356E 05	0.249726E 04	0.137776E 01	0.368356E 03	0.143906E 00
	0.176476E 05				
		0.000000E-38	0.264766E 04	0.110726E 01	0.931836E 04	0.143906E 02
		0.349686E 04	0.261146E 04	0.110956E 01	0.915306E 04	0.838036E 01
0.200006E 01					
	0.000000E-38				
		0.000000E-38	0.227956E 04	0.113236E 01	0.563436E 04	0.144006E 05
		0.390326E 04	0.224736E 04	0.113216E 01	0.531946E 04	0.778386E 04
		0.413486E 04	0.224366E 04	0.113226E 01	0.528026E 04	0.720006E 04
		0.499096E 04	0.222776E 04	0.113376E 01	0.511206E 04	0.514296E 04
		0.573476E 04	0.221226E 04	0.113696E 01	0.493386E 04	0.360006E 04
		0.573326E 04	0.221226E 04	0.122496E 01	0.493386E 04	0.360006E 04
		0.679006E 04	0.221226E 04	0.122956E 01	0.438126E 04	0.189476E 04
		0.944056E 04	0.221226E 04	0.126256E 01	0.249156E 04	0.106676E 03
		0.102846E 05	0.221226E 04	0.129556E 01	0.166496E 04	0.167446E 02
		0.103456E 05	0.221226E 04	0.129896E 01	0.160116E 04	0.141176E 02
		0.106656E 05	0.221226E 04	0.132006E 01	0.124076E 04	0.479966E 01
		0.111496E 05	0.221226E 04	0.136396E 01	0.503986E 03	0.143906E 00
	0.162506E 05				
		0.000000E-38	0.242016E 04	0.109656E 01	0.941106E 04	0.143906E 02
		0.333986E 04	0.238506E 04	0.109486E 01	0.927186E 04	0.844376E 01
0.225006E 01					
	0.000000E-38				
		0.000000E-38	0.219676E 04	0.112766E 01	0.565806E 04	0.144006E 05
		0.384396E 04	0.216426E 04	0.112506E 01	0.536066E 04	0.778386E 04
		0.407146E 04	0.216026E 04	0.112486E 01	0.532416E 04	0.720006E 04
		0.491616E 04	0.213366E 04	0.112406E 01	0.516946E 04	0.514296E 04
		0.565016E 04	0.212666E 04	0.112366E 01	0.500966E 04	0.360006E 04
		0.671636E 04	0.209886E 04	0.112496E 01	0.472936E 04	0.189476E 04
		0.671876E 04	0.209886E 04	0.121966E 01	0.472936E 04	0.189476E 04
		0.945466E 04	0.209886E 04	0.124766E 01	0.275166E 04	0.106676E 03
		0.103556E 05	0.209886E 04	0.127696E 01	0.187466E 04	0.167446E 02
		0.107626E 05	0.209886E 04	0.130076E 01	0.141706E 04	0.479966E 01
		0.111136E 05	0.209886E 04	0.134656E 01	0.710266E 03	0.287816E 00
	0.156776E 05	0.113966E 05	0.209886E 04	0.135376E 01	0.593416E 03	0.143906E 00
		0.000000E-38	0.233616E 04	0.109526E 01	0.941446E 04	0.143906E 02
		0.328136E 04	0.230236E 04	0.109326E 01	0.927816E 04	0.844376E 01
0.250006E 01					
	0.000000E-38				
		0.000000E-38	0.213056E 04	0.112616E 01	0.563786E 04	0.144006E 05
		0.378076E 04	0.209916E 04	0.112316E 01	0.534546E 04	0.778386E 04
		0.400446E 04	0.209536E 04	0.112286E 01	0.530966E 04	0.720006E 04
		0.483496E 04	0.207916E 04	0.112176E 01	0.515846E 04	0.514296E 04
		0.555706E 04	0.206026E 04	0.112086E 01	0.500286E 04	0.360006E 04
		0.660886E 04	0.203496E 04	0.112026E 01	0.473316E 04	0.189476E 04
		0.661036E 04	0.203496E 04	0.121796E 01	0.473316E 04	0.189476E 04
		0.931336E 04	0.203496E 04	0.124516E 01	0.276456E 04	0.106676E 03
		0.102046E 05	0.203496E 04	0.127356E 01	0.188986E 04	0.167446E 02
		0.106086E 05	0.203496E 04	0.129686E 01	0.143256E 04	0.479966E 01
		0.111566E 05	0.203496E 04	0.134356E 01	0.722256E 03	0.287816E 00
		0.112406E 05	0.203496E 04	0.135126E 01	0.604036E 03	0.143906E 00
	0.152026E 05				
		0.000000E-38	0.226546E 04	0.109476E 01	0.944066E 04	0.143906E 02
		0.326796E 04	0.223286E 04	0.109276E 01	0.927086E 04	0.844376E 01
0.300006E 01					
	0.000000E-38				
		0.000000E-38	0.203096E 04	0.112686E 01	0.553696E 04	0.144006E 05
		0.365656E 04	0.200306E 04	0.112496E 01	0.527136E 04	0.778386E 04
		0.387316E 04	0.199966E 04	0.112486E 01	0.520496E 04	0.720006E 04
		0.476776E 04	0.198546E 04	0.112446E 01	0.505036E 04	0.514296E 04
		0.553336E 04	0.197116E 04	0.112476E 01	0.488996E 04	0.360006E 04
		0.630486E 04	0.194776E 04	0.112726E 01	0.460066E 04	0.189476E 04
		0.917886E 04	0.189216E 04	0.120516E 01	0.321726E 04	0.106676E 03
		0.101676E 05	0.189036E 04	0.124676E 01	0.228116E 04	0.167446E 02
		0.107476E 05	0.189036E 04	0.124786E 01	0.228116E 04	0.167446E 02
		0.110256E 05	0.189036E 04	0.126746E 01	0.176656E 04	0.479966E 01
		0.112696E 05	0.189036E 04	0.131816E 01	0.934316E 03	0.287816E 00
		0.113656E 05	0.189036E 04	0.132916E 01	0.788636E 03	0.143906E 00
	0.194606E 05				
		0.000000E-38	0.215316E 04	0.107946E 01	0.943726E 04	0.143906E 02
		0.313506E 04	0.212296E 04	0.107306E 01	0.923596E 04	0.844376E 01

3.4 NOZZLE AND PLUME CALCULATION

Nozzle and plume calculations were performed as described in Section 2. Since the MOC program will handle only one shock wave at a time, the nozzle calculation was terminated when the internal shock intersected the axis. The problem was then inverted and the plume flow field was generated, using downstream shock points and nozzle exit plane points as a start line (Table 3). The plume was allowed to expand into a quasi-vacuum and the effects of the nozzle boundary layer were included. Because of the large expansions encountered, a characteristic mesh control was imposed on the solution to prevent divergence problems. The maximum mesh size permitted was 20 in. measured along any side of a Mach quadralateral. The effect of the boundary layer was to cause a greater expansion due to the lower lip Mach number of the boundary layer.

Table 3

PLUME STARTING LINE PROPERTIES

STARTING LINE

R	X	M	THETA	S	O/F
.00000	.81706+01	.41359+01	.16411+02	.10427+04	.30600+01
-.70000-02	.81620+01	.42700+01	.14600+02	.81700+03	.30582+01
-.14000-01	.81500+01	.43750+01	.13200+02	.66100+03	.30563+01
-.23500-01	.81240+01	.44800+01	.11800+02	.51800+03	.30532+01
-.37500-01	.80830+01	.45908+01	.10400+02	.38600+03	.30479+01
-.60428-01	.80076+01	.46893+01	.91554+01	.28294+03	.30455+01
-.90000-01	.79130+01	.47679+01	.82030+01	.22200+03	.30305+01
-.14052+00	.77304+01	.48488+01	.68893+01	.14956+03	.30248+01
-.19276+00	.75304+01	.48683+01	.55979+01	.11046+03	.30112+01
-.24391+00	.73205+01	.48688+01	.45458+01	.85964+02	.29975+01
-.34186+00	.69167+01	.48262+01	.25844+01	.53456+02	.29663+01
-.53038+00	.71480+01	.47852+01	.11371+01	.24516+02	.28858+01
-.67852+00	.70674+01	.47374+01	.65649-01	.14420+02	.28250+01
-.83143+00	.71190+01	.47533+01	-.12933+01	.83803+01	.27606+01
-.97760+00	.70997+01	.47467+01	-.22685+01	.46639+01	.26959+01
-.11880+01	.70702+01	.46834+01	-.34540+01	.16392+01	.25916+01
-.13991+01	.69650+01	.46024+01	-.45319+01	.35095+00	.24721+01
-.15127+01	.69725+01	.45822+01	-.51954+01	.11745+00	.23927+01
-.16358+01	.69577+01	.45833+01	-.59645+01	.39184-01	.23098+01
-.18238+01	.68801+01	.44650+01	-.60597+01	.72613-01	.21620+01
-.20609+01	.69246+01	.44292+01	-.68417+01	.11828-02	.19626+01
-.22664+01	.68455+01	.43463+01	-.74834+01	.25112-03	.17571+01
-.25993+01	.69840+01	.41885+01	-.76787+01	.32927-02	.12800+01
-.26085+01	.69840+01	.37795+01	-.76787+01	.16924+04	.12800+01
-.26174+01	.69840+01	.34529+01	-.76787+01	.31139+04	.12800+01
-.26261+01	.69840+01	.31800+01	-.76787+01	.43332+04	.12800+01
-.26345+01	.69840+01	.29475+01	-.76787+01	.53954+04	.12800+01
-.26426+01	.69840+01	.27428+01	-.76787+01	.63319+04	.12800+01
-.26504+01	.69840+01	.25602+01	-.76787+01	.71655+04	.12800+01
-.26580+01	.69840+01	.23954+01	-.76787+01	.79131+04	.12800+01
-.26653+01	.69840+01	.22450+01	-.76787+01	.85876+04	.12800+01
-.26723+01	.69840+01	.21065+01	-.76787+01	.91991+04	.12800+01
-.26791+01	.69840+01	.19781+01	-.76787+01	.97557+04	.12800+01
-.26855+01	.69840+01	.18583+01	-.76787+01	.10264+05	.12800+01
-.26917+01	.69840+01	.17454+01	-.76787+01	.10729+05	.12800+01
-.26977+01	.69840+01	.16384+01	-.76787+01	.11156+05	.12800+01
-.27033+01	.69840+01	.15368+01	-.76787+01	.11547+05	.12800+01
-.27087+01	.69840+01	.14397+01	-.76787+01	.11907+05	.12800+01
-.27138+01	.69840+01	.13605+01	-.76787+01	.12238+05	.12800+01
-.27186+01	.69840+01	.12724+01	-.76787+01	.12542+05	.12800+01
-.27232+01	.69840+01	.11868+01	-.76787+01	.12821+05	.12800+01
-.27274+01	.69840+01	.11036+01	-.76787+01	.13076+05	.12800+01

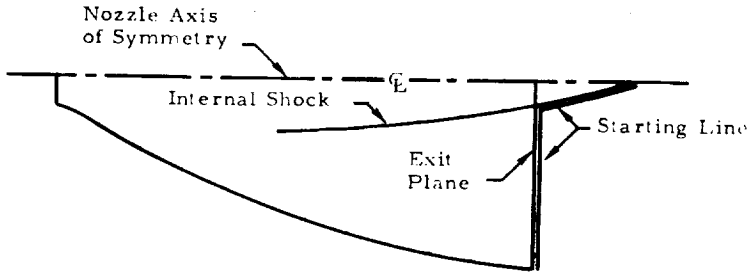

Section 4
PRESENTATION OF RESULTS

4.1 DISCUSSION OF RESULTS

The results of the study are presented in terms of plume parameters as a function of spatial location, i.e., contour plots, as well as centerline property distributions within the plume. Tables of thermochemical properties used in the generation of the plume are also presented.

The distribution of mass flow in the plume is shown in Fig. 6. Each streamline represents a percentage of the total mass flow contained in the region between the streamline and the centerline. Contour maps of the plume properties, i.e., Mach number, temperature, pressure, density, flow angle, pitot pressure and O/F ratio are presented in Figs. 7 through 13. It can be seen that these contour plots are not the smooth patterned curves normally presented for plume calculations. It should be recalled, however, that in keeping with the study objective, every calculable effect was taken into account in generating the detailed plume properties presented herein. It is not surprising, therefore, to expect slight irregularities in the contour plots arising from such effects as O/F gradients, entropy gradients (due to shock waves), nozzle wall boundary layer, and the nozzle contour itself, which gives rise to additional compressions in the flow field.

In addition to the contour maps, plots of the centerline distributions of the plume parameters are presented in Figs. 14 through 17. The pitot pressures presented in Fig. 15 should aid in comparing experimental data which usually consists of pitot pressure measurements along the centerline.

As discussed in Section 2.4.1, continuum analyses were used throughout the flow field. To obtain an indication of where non-continuum effects may

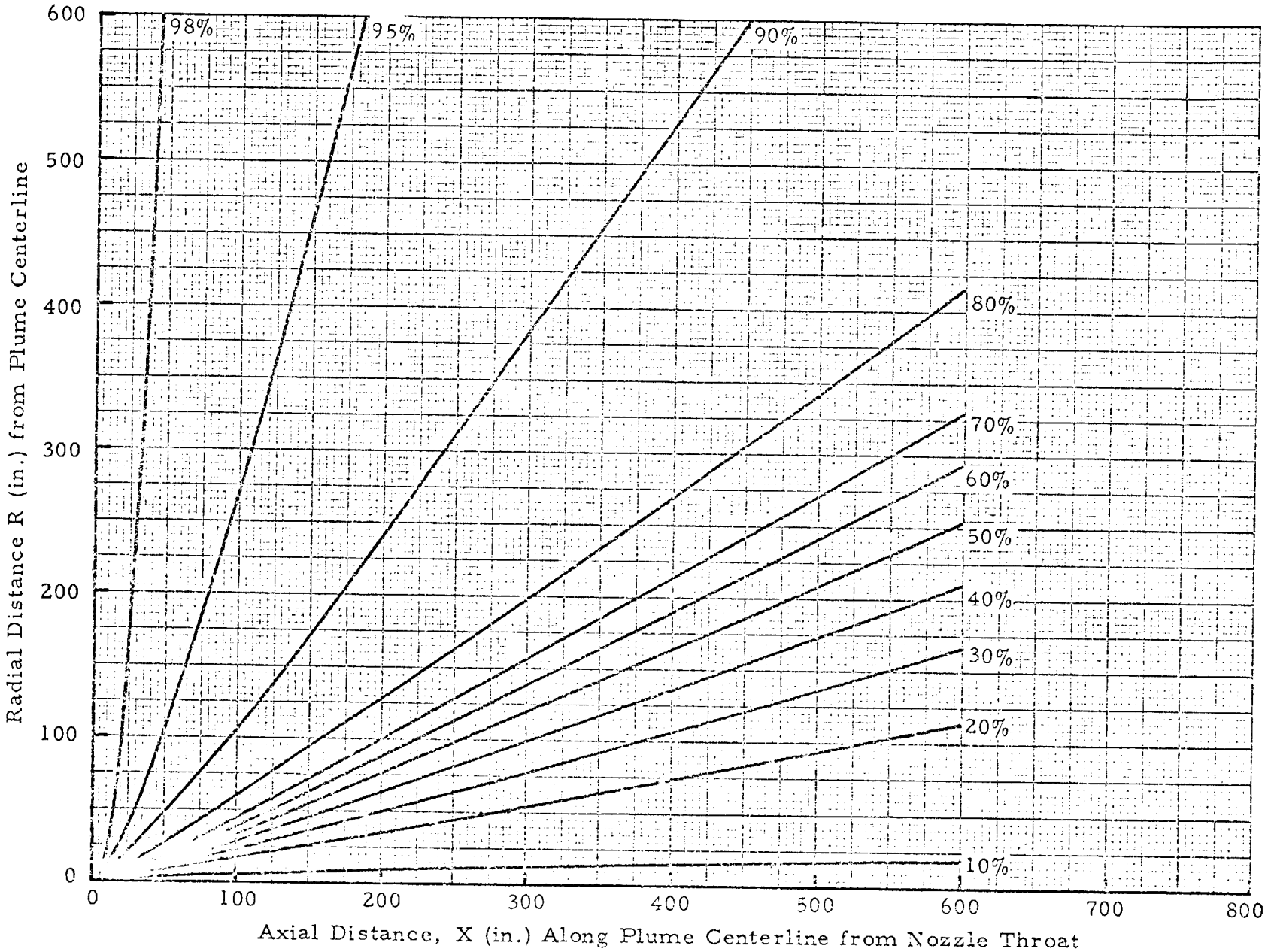

Fig. 6 - Location of Streamlines and Mass Flow Distribution (Percent of Total) in R-4D Plume Flowfield

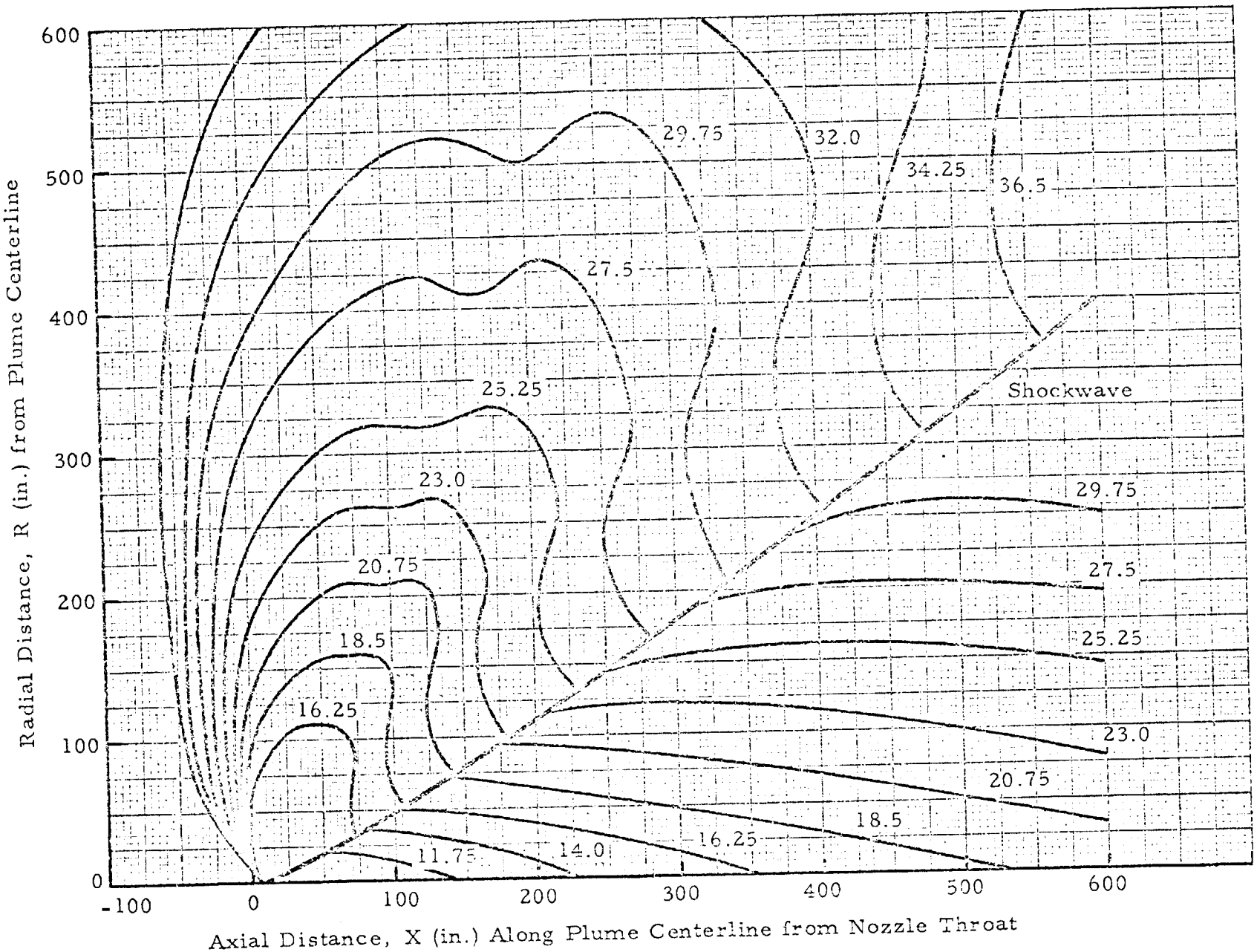

Fig. 7 - Lines of Constant Mach Number in R-4D Plume Flowfield

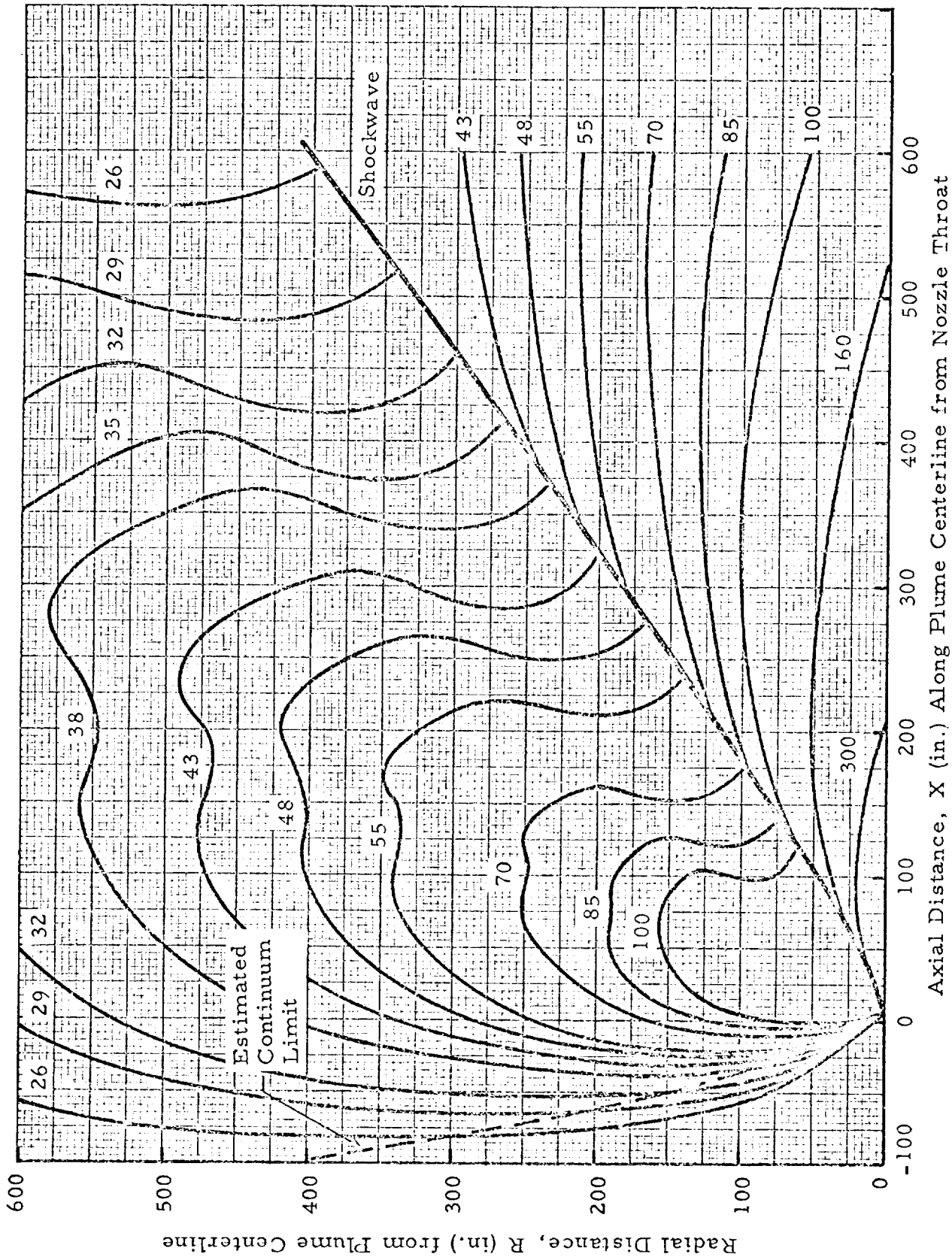

Fig. 8 - Lines of Constant Temperature (^{o}R) in R-4D Plume Flowfield

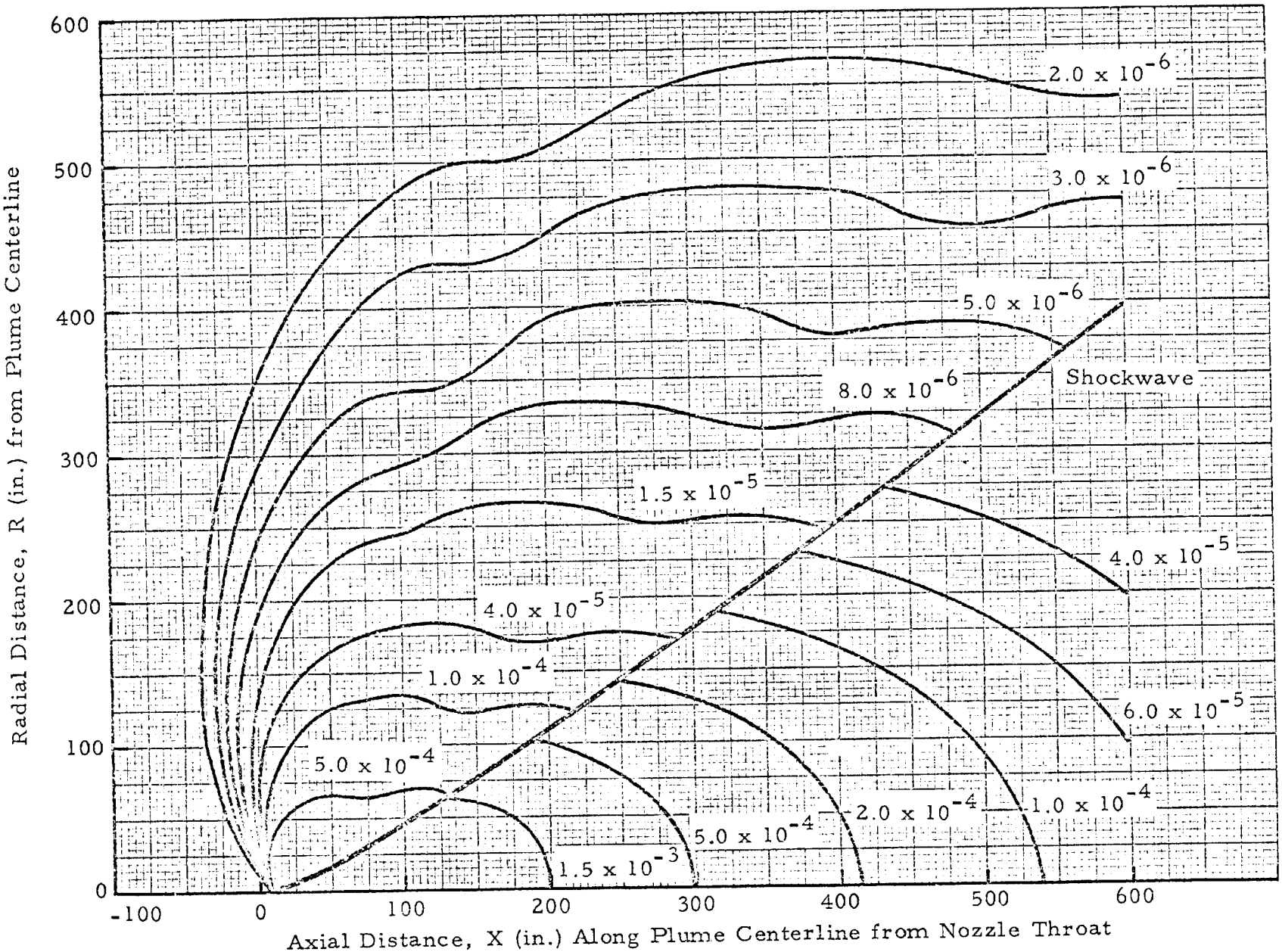

Fig. 9 - Lines of Constant Static Pressure (psfa) in R-4D Plume Flowfield

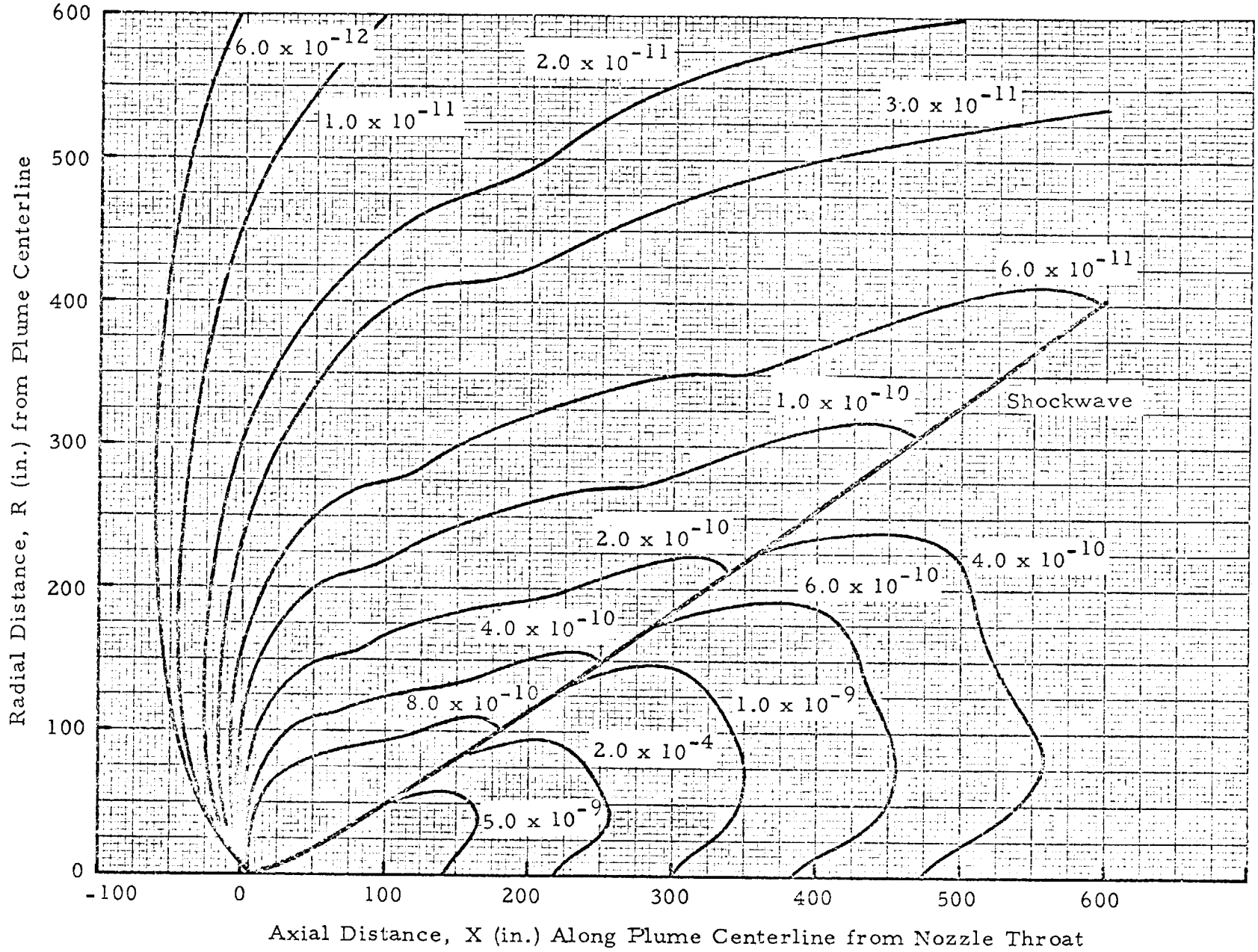

Fig. 10 - Lines of Constant Density (slugs/ft^3) in R-4D Plume Flowfield

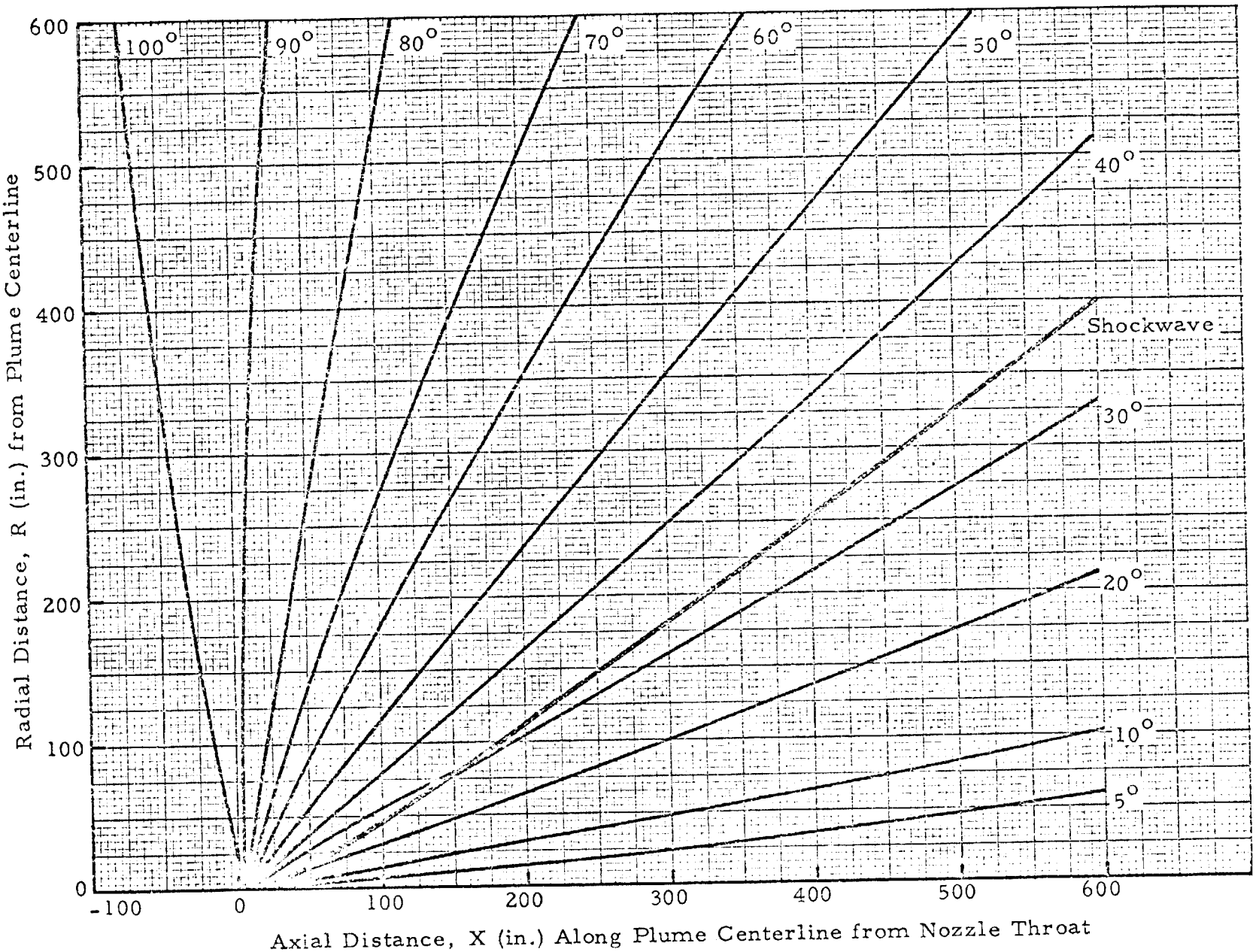

Fig. 11 - Lines of Constant Flow Angle (degrees) in R-4D Plume Flowfield

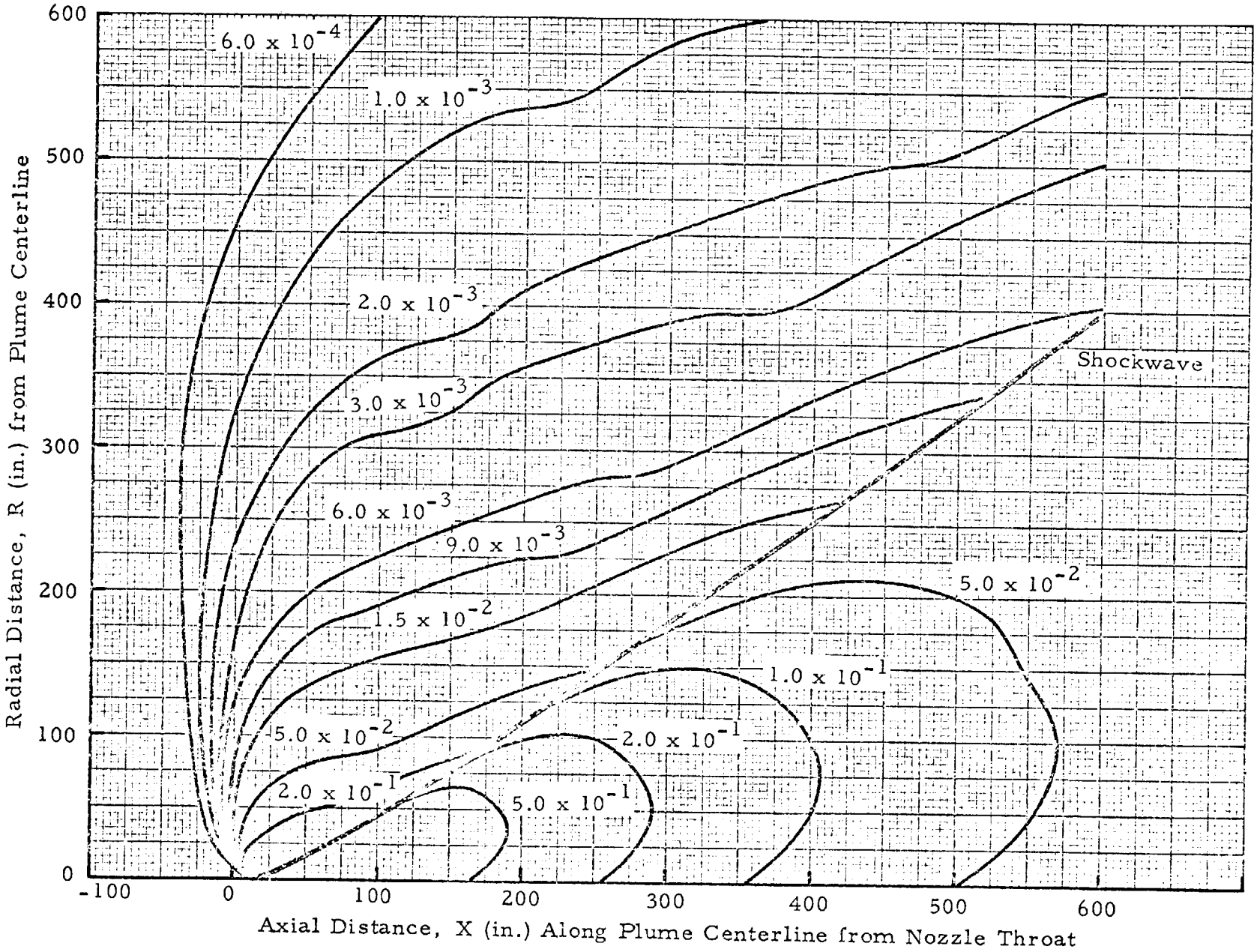

Fig. 12 - Lines of Constant Pitot Pressure (psfa) in the R-4D Plume Flowfield

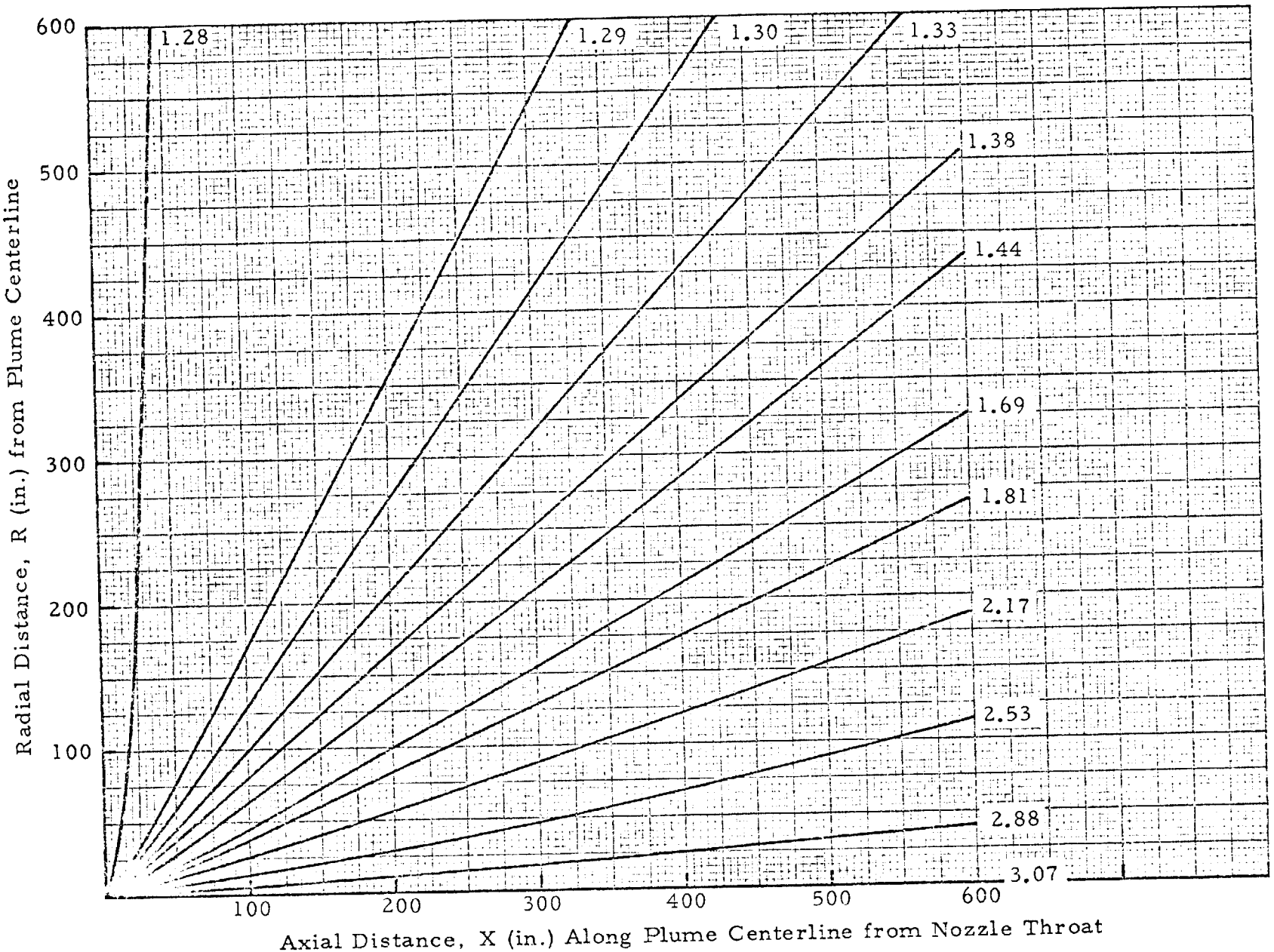

Fig. 13 - Lines of Constant O/F Ratio in R-4D Plume Flowfield

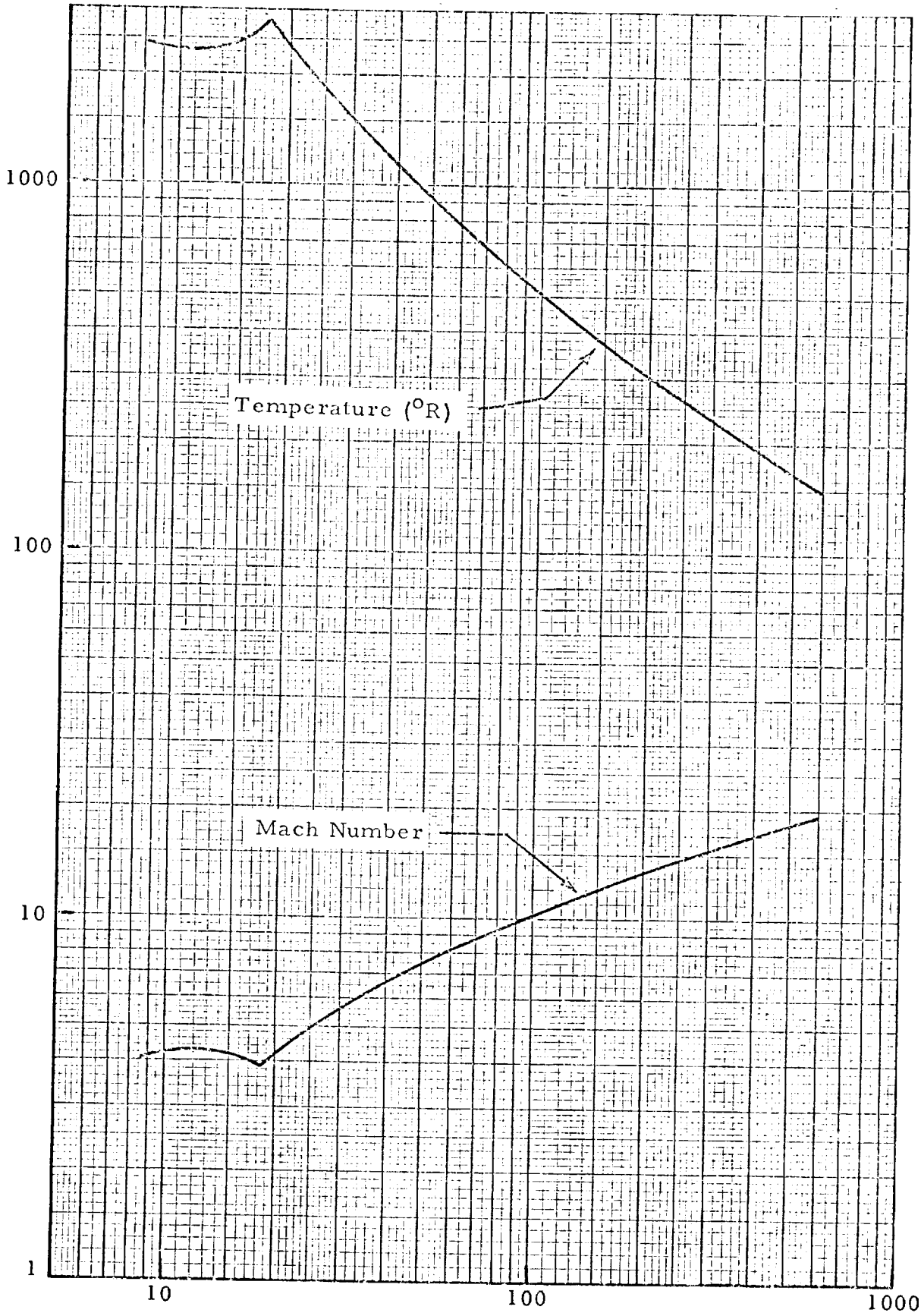

Fig. 14 - Mach Number and Temperature Distribution Along Centerline of R-4D Plume Flowfield

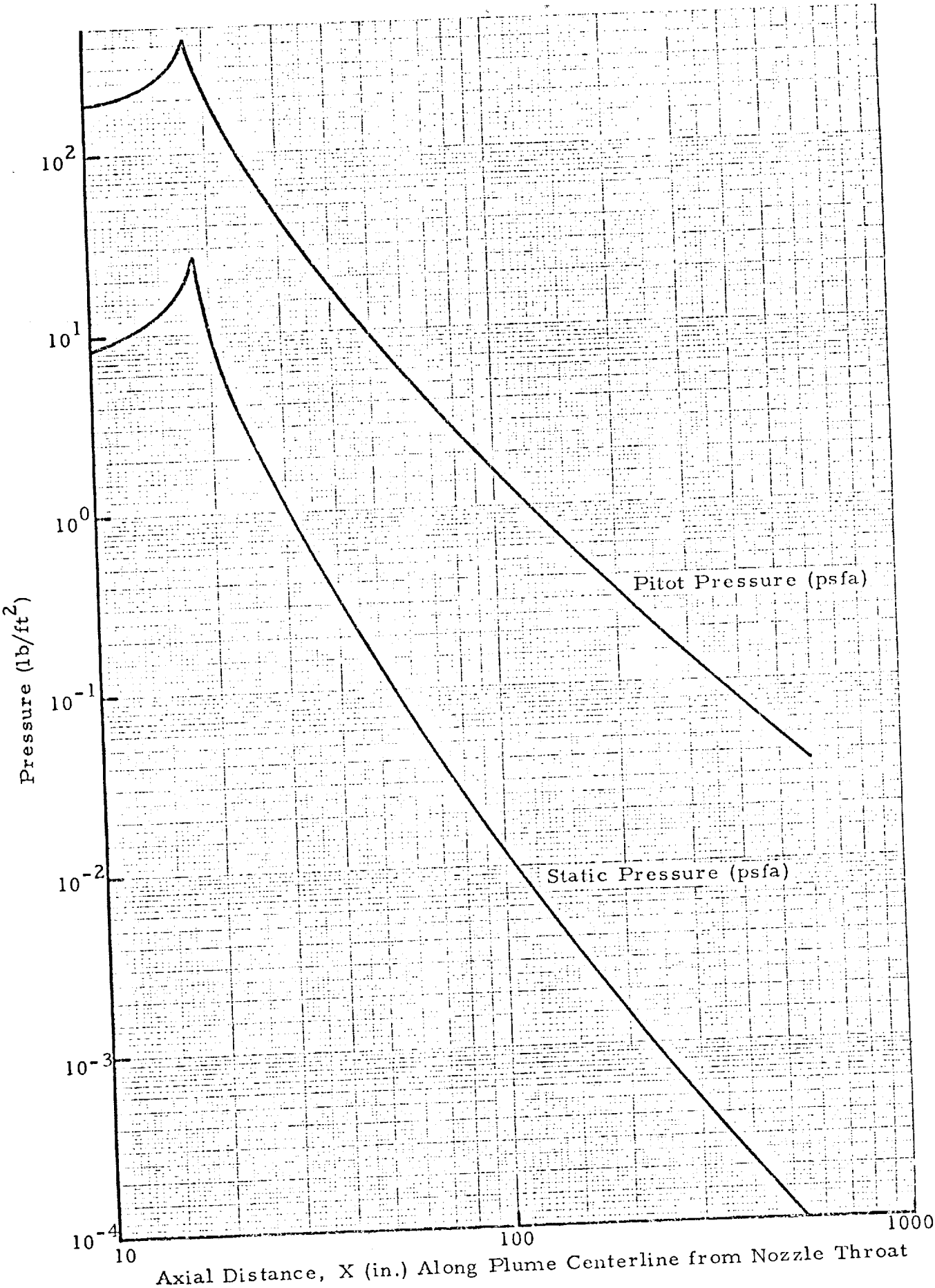

Fig. 15 - Pitot and Static Pressure Distribution Along Centerline of R-4D Plume Flowfield

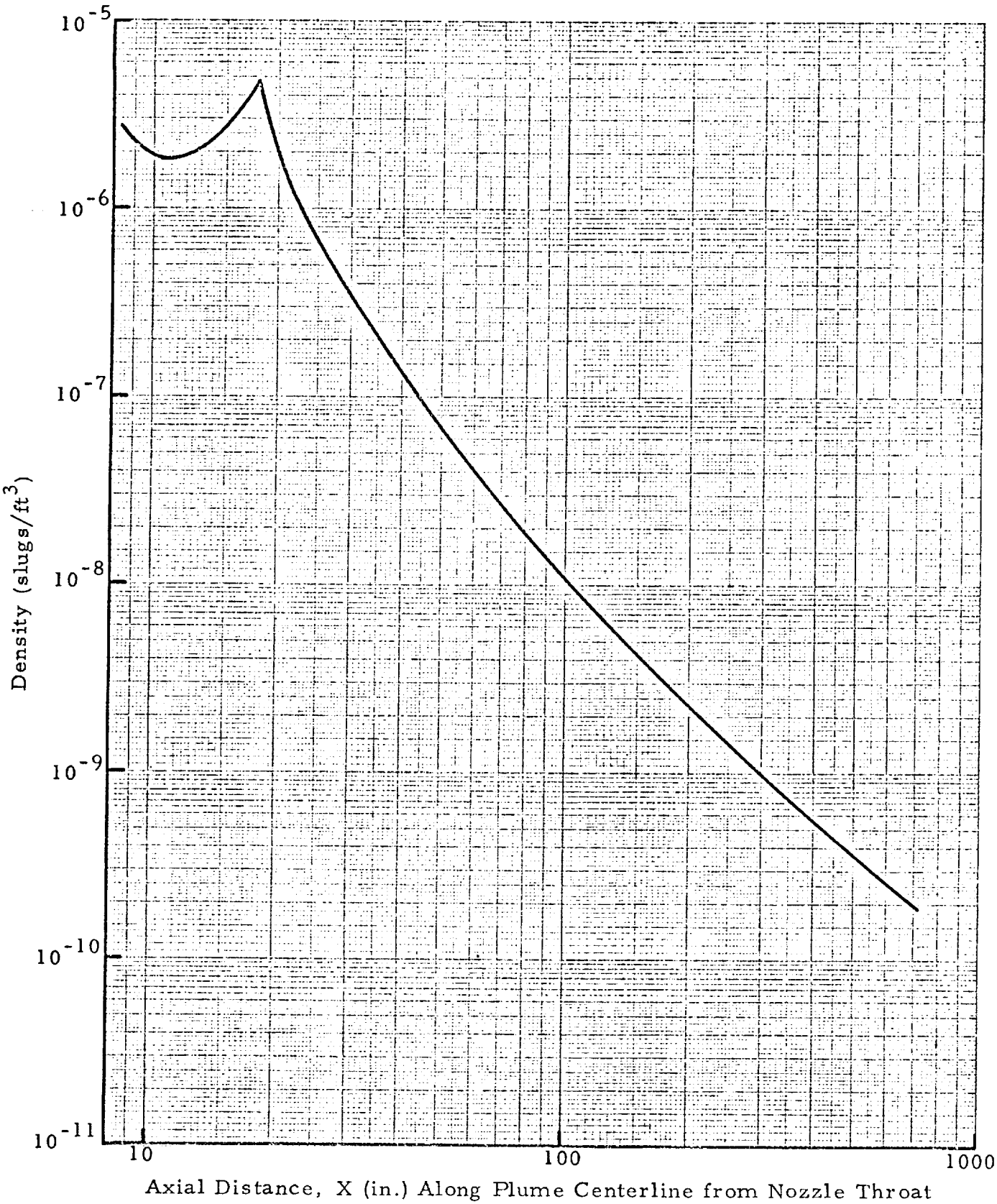

Fig. 16 - Density Distribution Along Centerline of R-4D Plume Flowfield

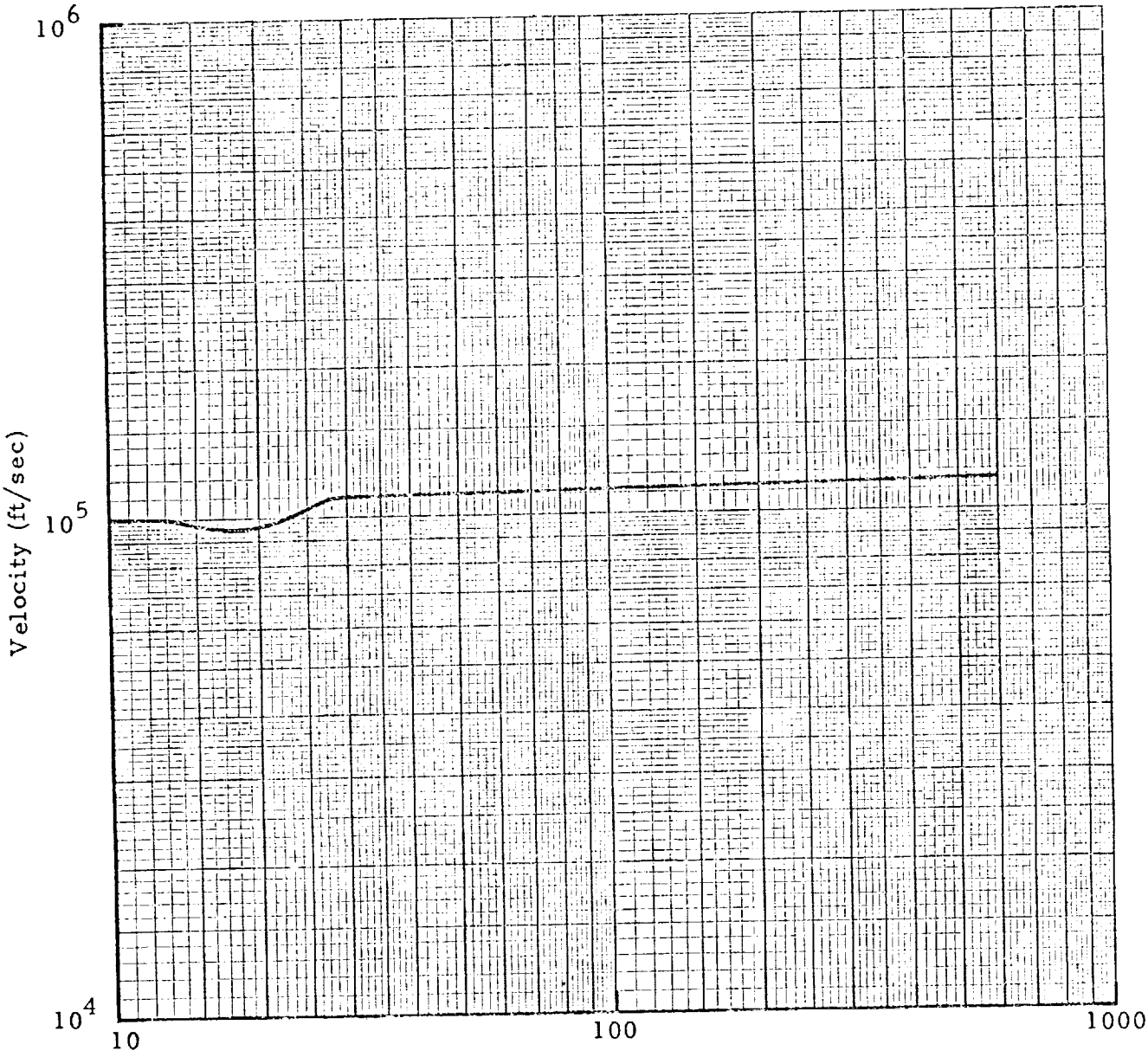

Fig. 17 - Velocity Distribution Along Centerline of R-4D Plume Flowfield

become detectable, however, the translational "freeze" line based on a Knudsen number criterion of 1.0 was computed and is shown on the temperature contour plot, Fig. 8. The major deviation caused by non-continuum effects would be in the streamwise temperature component which would be somewhat higher, in the region above the "freeze" line, than the continuum calculations shown in Fig. 8.

Since the kinetics analysis, previously discussed, indicated that the flowfield chemistry was frozen inside the nozzle, the entire plume was computed using frozen chemistry. The species present in the plume as a function of O/F ratio are presented in Table 4.

4.2 SUMMARY OF RESULTS

The plume flow field of the R-4D motor was analytically generated, the analysis starting at the injector and continuing through the combustion chamber, the subsonic and supersonic nozzle sections, and 50 feet into the plume region. To provide the basic information needed for doing impingement analyses, the plume data were generated to be as detailed as possible including all the existing calculation procedures to treat the physical phenomena present. The momentum loss because of combustion, O/F maldistribution, kinetic effects and two-dimensional effects which cause non-ideal engine performance were treated as integral parts of the analysis. The possibility of condensation was considered but incipient condensation or calculation of a multi-phase plume flow field was not treated in this analysis. The effect on the plume flow field of nozzle boundary layer and internal shocks appeared in the plots of physical properties of the plume. While the plots of the flow properties contain certain irregularities not present in a more simplified plume analysis, these irregularities were found to be present when every calculable effect in the flow was treated in generating the plume properties. When detailed impingement analyses are required, the inclusion of all the calculable effects was therefore concluded to be necessary and worthy of the increased time and effort.

Table 4

CONSTITUENT MOLE FRACTIONS AT THE FREEZING POINT PRESSURES FOR THE R-4D ENGINE NOZZLE FLOW WITH AN O/F VARIATION FROM 1.24 TO 3.07 WITH AN N_2O_4/MMH PROPELLANT SYSTEM

O/F Ratio	1.240	1.290	1.300	1.330	1.380	1.440
CO	0.15345	0.15204	0.15147	0.14975	0.14674	0.14294
CO_2	0.02404	0.02462	0.02501	0.02619	0.02829	0.03099
H	0.00256	0.00440	0.00458	0.00516	0.00615	0.00748
H_2	0.28853	0.27303	0.26958	0.25927	0.24241	0.22262
H_2C	0.24250	0.25436	0.25717	0.26547	0.27893	0.29439
NO	0.00002	0.00005	0.00005	0.00007	0.00010	0.00016
N_2	0.28857	0.29074	0.29133	0.29307	0.29594	0.29926
O	0.00000	0.00001	0.00001	0.00001	0.00002	0.00005
OH	0.00032	0.00074	0.00079	0.00100	0.00140	0.00207
O_2	0.00000	0.00000	0.00000	0.00001	0.00001	0.00003

O/F Ratio	1.636	1.814	2.170	2.526	2.882	3.070
CO	0.12861	0.11302	0.07754	0.04338	0.00860	0.00000
CO_2	0.04160	0.05360	0.08144	0.10778	0.13617	0.14272
H	0.01163	0.01408	0.01255	0.00695	0.00099	0.00000
H_2	0.16313	0.11803	0.05766	0.02607	0.00507	0.00000
H_2O	0.33876	0.36910	0.40147	0.41113	0.42282	0.42815
NO	0.00062	0.00155	0.00462	0.00695	0.00482	0.00014
N_2	0.30933	0.31720	0.32940	0.33886	0.35127	0.35705
O	0.00027	0.00087	0.00320	0.00443	0.00161	0.00000
OH	0.00582	0.01141	0.02301	0.02559	0.01182	0.00004
O_2	0.00023	0.00112	0.00912	0.02885	0.05682	0.07190

REFERENCES

1. Ratliff, A. W., and J. T. Stephens, "A Detailed Plume Flowfield Definition of the R-1E Motor for the Saturn S-IVB Auxiliary Propulsion System," LMSC/HREC D148776, Lockheed Missiles & Space Company, Huntsville, Ala., June 1969.

2. Prozan, R. J., "Striated Combustion Solution," LMSC/HREC A791356, Lockheed Missiles & Space Company, Huntsville, Ala., May 1968.

3. Letter to Mr. David Seymour (NASA-Marshall Space Flight Center) from Dr. Raymond Edelman (General Applied Science Laboratories) 29 October 1968.

4. Prozan, R. J., "Development of a Method-of-Characteristics Solution for Supersonic Flow of an Ideal, Frozen, or Equilibrium Reacting Gas Mixture," LMSC/HREC D782535-A, Lockheed Missiles & Space Company, Huntsville, Ala., April 1966.

5. McBride, Bonnie, and Sanford Gordon, "Preliminary Description of CEC, A Computer Program for the Calculation of Chemical Equilibrium Compositions with Applications," NASA-Lewis Research Center, Cleveland, Ohio, 31 May 1968.

6. Komianos, S. A., G. D. Bleich and H. S. Pergament, "The AeroChem Nonequilibrium Streamline Program," AeroChem TN-103, AeroChem Research Laboratories, Inc., Princeton, N. J., May 1967.

7. Golden, J. O., and L. W. Spradley, "Description of a Digital Computer Code for Rocket Nozzle Sudden Freezing Analyses," LMSC/HREC A784526, Lockheed Missiles & Space Company, Huntsville, Ala., July 1967.

8. Robertson, S. J., "A Method for Calculating Flowfield Properties in Low Density Plumes," LMSC/HREC A784697, Lockheed Missiles & Space Company, Huntsville, Ala., October 1967.

9. Boynton, F. P., "Exhaust Plumes from Nozzles with Wall Boundary Layers," J. Spacecraft Roc., Vol. 5, October 1968, pp 1143 - 1147.

10. Smith, S. D., and A. W. Ratliff, "A Study of the Effect of a Boundary Layer along a Nozzle Wall on the Plume Flow Field," LMSC/HREC D149477, Lockheed Missiles & Space Company, Huntsville, Ala., 12 January 1970.

11. Ratliff, A. W., and J. W. Benefield, "Estimation of Accuracy of Rocket Exhaust Plume Flowfield Variables," LMSC/HREC A791939, Lockheed Missiles & Space Company, Huntsville, Ala., 2 July 1969.

12. Pieper, J. L., "ICRPG Liquid Propellant Thrust Chamber Performance Evaluation Manual," CPIA No. 178, Chemical Propulsion Information Agency, September 1968.

13. Audeh, B. J., "Effect of Freezing-Point Location on Specific Impulse Prediction," LMSC/HREC D149246, Lockheed Missiles & Space Company, Huntsville, Ala., October 1969.

Appendix A

SUPPLEMENTARY STUDY OF THE R-4D ENGINE USING N_2O_4/A-50 PROPELLANTS

Appendix A

A.1 INTRODUCTION

During study of the RCS motors for the Skylab configuration, experimental data from tests conducted at Manned Spacecraft Center (MSC) were used to help verify the analytical techniques and assumptions employed in the calculational scheme. Unfortunately, the test results were for an RCS engine (R-4D) using N_2O_4/A-50 propellants, whereas the Skylab configuration RCS engines utilize N_2O_4/MMH propellants. Nevertheless, it was deemed necessary to perform these correlations in order to determine the appropriate mixture ratio variation, since the engines are identical and only the propellants differ.

The experimental data indicated the presence of strong oxidizer-to-fuel-ratio (O/F) gradients and this fact was verified by injector mass flow and O/F distribution information received from the Marquardt Corporation. The experimental specific impulse (I_{sp}) was much lower than that computed by conventional means, also indicating the presence of O/F gradients, perhaps coupled with combustion inefficiency. Thus, a preliminary step in the study was to determine an appropriate O/F ratio gradient which would not only predict the I_{sp} more accurately, but would also correlate the experimental measurements of pitot pressure and heating rates across the plume near the exit plane of the nozzle.

A.2 DISCUSSION

A.2.1 Background

There were two basic measurements available, (1) pitot pressure and (2) stagnation point heating rate data from surveys made across the plume

near the exit plane and at several stations downstream of the exit. In addition, a measure of the engine efficiency was available by way of the I_{sp}. Initial effort directed toward determining the O/F ratio profile consisted of a two-pronged approach. Since the incoming or overall O/F ratio was known, it was used as a basic constraint on the system and the O/F profile at the nozzle throat was perturbed until the best fit of the pitot pressure data at the exit plane was obtained. Using the O/F ratio distribution determined in that manner, the I_{sp} was then examined to see if it was in line with the experimental value. The other approach (and the one which was ultimately selected due to its more fundamental nature) was based upon an analysis beginning at the injector face and proceeding throughout the engine. This approach accounts for mixing and burning between the various streams of differing O/F ratio in the combustion chamber as well as the two-dimensional effects in the transonic region. The supersonic expansion region was treated by the method of characteristics as in the preceeding approach.

A.2.2 Detailed Calculations

The O/F ratio distribution was determined from injector information and the assumption of constant mass flow per unit area. The centerline O/F value was fixed at the O/F ratio of the preigniter and the wall O/F value was determined from the overall O/F ratio, assuming a parabolic profile. These assumptions resulted in a distribution described by the following expression

$$\eta = 3.5 - 3.76\, r^2 ,$$

where η is the O/F ratio and r is the radial coordinate in inches at the injector.

Following the calculational scheme previously outlined, the engine nozzle and plume flowfield was computed. Correlations with experimental pitot pressures available are shown in Figs. A-1 through A-3. Figure A-4 shows the correlation for the stagnation point heating rate values.

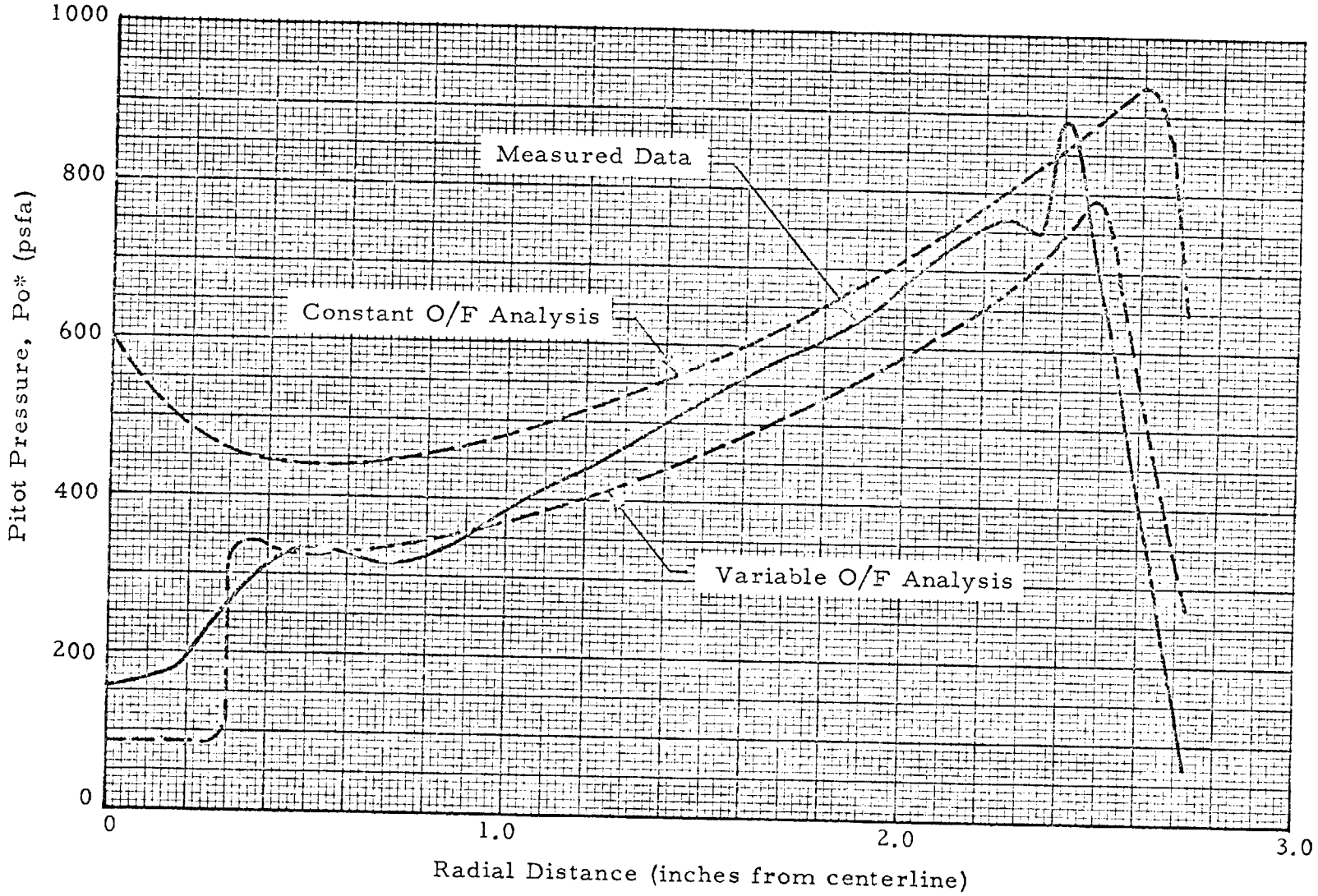

Fig. A-1 - Comparison of Measured and Calculated Pitot Pressures One-Half Inch Downstream of Exit Plane

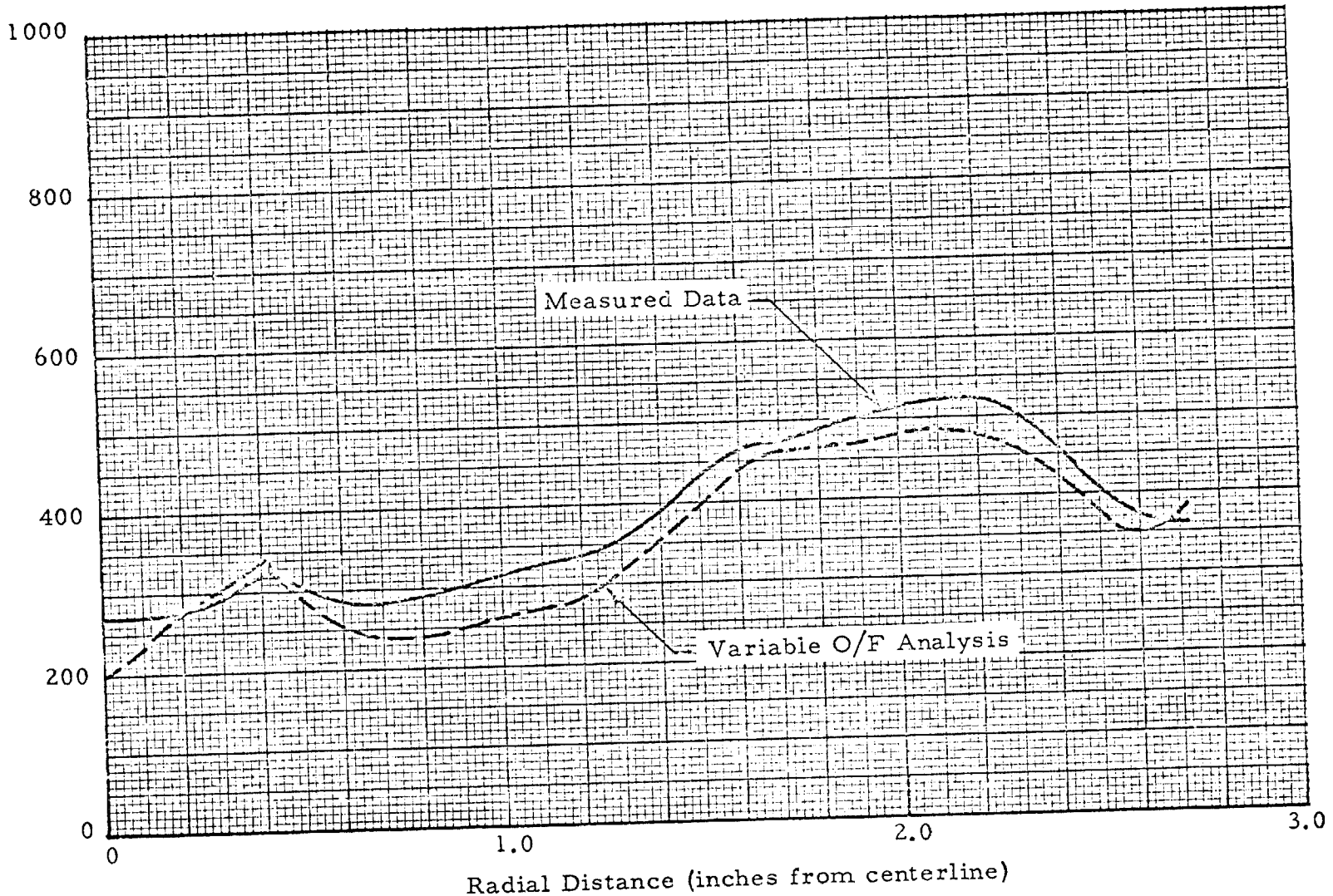

Fig. A-2 - Comparison of Measured and Calculated Pitot Pressures Three and One-Half Inches Downstream of Exit Plane

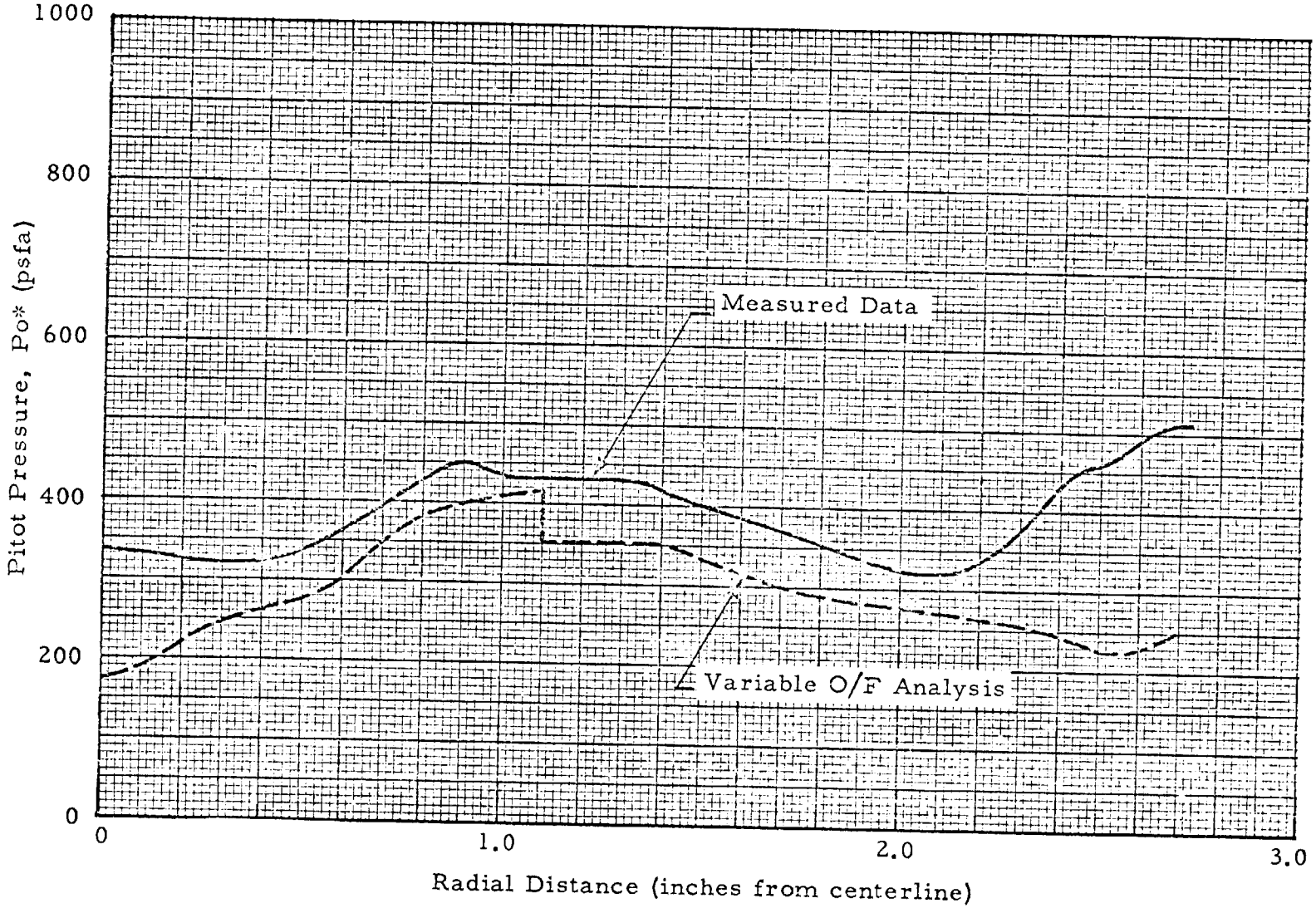

Fig. A-3 - Comparison of Measured and Calculated Pitot Pressures Six and One-Half Inches Downstream of Exit Plane

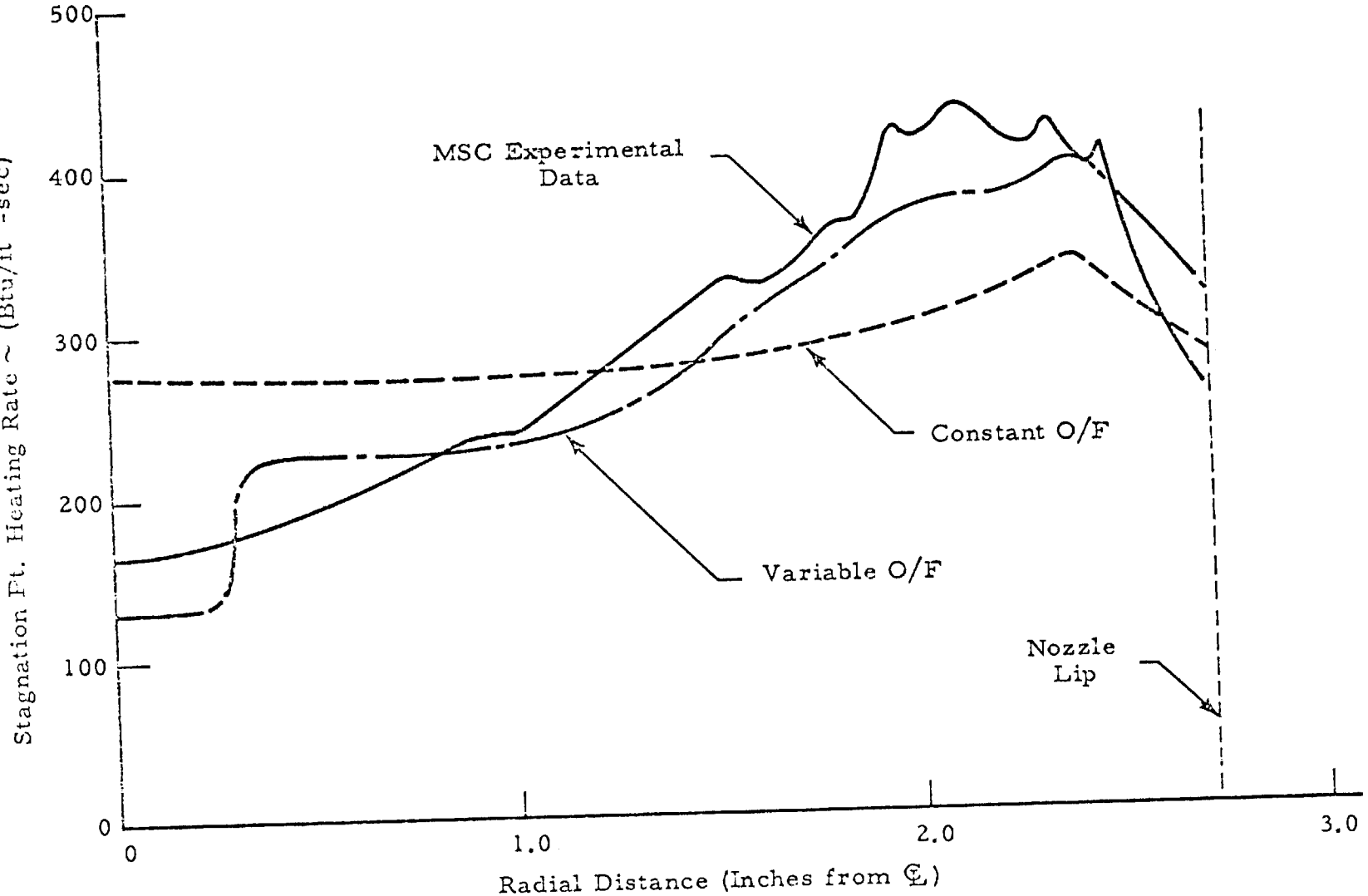

Fig. A-4 - Radial Heating Rate Variation 2.5 Inches From Exit Plane

In Fig. A-1 the measurements and calculations are for a plane 1/2-in. downstream of the nozzle exit. This figure shows the solution obtained from a non-distributed O/F ratio calculation fixed at a constant value of 2.0. As can be seen, the correlation, which assumes a constant O/F ratio is reasonable near the nozzle lip, but deviates quite badly near the centerline. Results from the distributed O/F ratio calculation also plotted on Fig. A-1 show significant improvement in the correlation, especially near the axis.

Some comment is in order concerning the relationship between the pitot pressure correlation near the centerline and the location of the shock wave generated by the reflex nozzle contour. The constant O/F ratio analysis does not even come close to predicting the proper shock location, whereas the distributed O/F ratio result correlates quite well. The measured pitot pressure data was noted to drop rapidly near the nozzle lip (the data were taken 1/2-in. downstream of the nozzle exit plane). The conclusion might be reached that this effect is due entirely to the nozzle lip expansion fan, but the analysis shows that this region is not greatly affected by the fan, but is actually altered greatly by the value of O/F ratio used at the wall. This effect is exemplified by comparing the pitot pressures near the nozzle lip. The constant O/F ratio value of 2.0, produces pitot pressures which are a factor of two higher than those predicted by the variable O/F ratio analysis along the streamline whose O/F ratio is 1.2. Here, of course, the variable O/F ratio result is much closer to the experimental value.

As previously mentioned, the measured I_{sp} was much lower than the constant O/F ratio prediction. The predicted I_{sp} using a constant O/F ratio analysis at the incoming mixture ratio value of 2.0 was 340 lb_f-sec/lb_m where the measured I_{sp} was 280 to 285 lb_f-sec/lb_m. The mixture ratio variation used in this analysis resulted in an I_{sp} prediction of about 300 lb_f-sec/lb_m, which means, of course, that in addition to the mixture ratio variation, there must also be some combustion inefficiency to account for the remainder of the performance degradation.

By arbitrarily reducing the propellant heats of formation, exactly the right I_{sp} can be produced; however, the objective of this study was not to predict performance but rather to describe the plume properties. Reducing propellant heats of formation had relatively little effect on correlating pitot pressure. The analytical curve tended to shift toward the centerline but its magnitude was not significantly altered. Since the plume property data will be used to design the vehicle, the data was generated without arbitrarily reducing the heats of formation in order to predict conservative design numbers.

Figures A-2 and A-3 present pitot pressure correlations at two other downstream stations and, as can be seen, the comparison is quite good, indicating that the analysis procedure utilized is applicable. In Fig. A-4 a comparison of the heating rates at a station $2\frac{1}{2}$-in downstream of the exit plane is shown. Without going into detail about the heating rate calculations note that the same procedure was used in calculating both the constant and the variable O/F ratio values so that any difference in the correlation is due strictly to the O/F gradient.

A.3 CONCLUSIONS

This auxiliary R-4D engine study was carried out, at least in part, to verify the analytical technique utilized for the study reported in the main body of this document. Comparison with measured pitot pressures, heating rates and performance parameters have shown that the procedure is quite adequate.

MSFC—RSA, Ala